Open Access

IJCER ONLINE

ISSN Online: 2250–3005

Impact Factor: 1.145

IJCER - International Journal of Computational Engineering Research

Volume 05 – Issue 08, (August 2015)

www.ijceronline.com– Email–ijceronline@gmail.com

Editorial Board

Editor-In-Chief

Editorial Committees

Contents:

ISSN (e): 2250 – 3005 || Volume, 05 || Issue, 08 ||August – 2015 ||
International Journal of Computational Engineering Research (IJCER)

A Study on Biological Treatment of Bio-Diesel Industrial Effluent Using FBBR

Dr.G.V.R.Srinivasa Rao[1], K.Srinivasa Murty[2], J.Chiranjeevi[3]
[1](Professor, Dept. of Civil Engineering,Andhra Univesity,Visakhapatnam)
[2] (Lecturer,MRAGR Govt.Polytechnic, Vizianagaram)
[3](PG Student,Dept of Civil Engg., Andhra University, Visakhapatnam)

Abstract:
The present study involves experimentation on the treatment of bio-diesel industrial effluent using a laboratory scale model of Fluidized Bed Bioreactor (FBBR) with three different bed materials viz., MBBR Plastic media, Pumice Stones, high density Foam material. The experiment mainly focuses on the removal of Biological Oxygen Demand (BOD) and Chemical Oxygen Demand (COD) from the bio-diesel industrial effluent. The experiment is conducted for a period over 2 to 3 weeks at daily intervals, till the reactor gets stabilized and a maximum and uniform rates of percent removal of BOD and COD are obtained. The experimental data is analyzed and the results are presented in suitable formats. From the Bio-kinetic study involving reaction rate kinetics and microbial growth kinetics it is observed that, the bio-kinetic reactions taking place in the reactor conform to First order rate of reactions and the Foam pieces are proved to be a good alternative material when compared with that of the Commercially available MBBR (plastic) media.

Keywords: *Bed material, Biological Oxygen Demand (BOD), Bio-diesel, Chemical Oxygen Demand (COD), Fluidized Bed Bio Reactors (FBBR), Microbial Growth Kinetics, Reaction rate kinetics.*

I. Introduction

Biodiesel is a domestically produced renewable fuel that can be manufactured from vegetable oils, animal fats or recycled organic materials like greases etc. Most biodiesel manufacturing processes result in the generation of process effluents with free fatty acids and glycerin. Other constituents in the biodiesel industrial effluent include organic residues such as esters, soaps, inorganic acids and salts, traces of methanol etc. The typical biodiesel manufacturing process effluent has high concentrations of BOD, COD, TSS, oil and grease etc. The present work focuses on the removal of BOD and COD from the effluents generated in the bio-diesel industry using a laboratory scale Fluidized Bed Bioreactor (FBBR). Earlier works on FBBR have reported good removal of organic wastes[1,2] and a good number of empirical as well as rational parameters based on biological kinetic equations can be used in the design of biological wastewater treatment processes like FBBR [3]. These Bio-kinetic coefficients include specific growth rate (μ), maximum rate of substrate utilization per unit mass of microorganisms (k), half velocity constant (k_s), maximum cell yield (Y) and endogenous decay coefficient (k_d) and to be used in the design of bio-reactors [4]

II. Experimental Setup

The experimental system consists of three Acrylic glass columns of 120 cm length and 6.9 cm dia each arranged parallel to each other, with valves at the top and bottom of the columns to regulate the flow through them, as shown in Fig.1. The columns are filled with different bed materials viz., Commercially available MBBR (Plastic) media, Pumice stones and high density Foam pieces. A mesh is provided between the flanges so as to prevent the loss of bed material into the pipe. A flow meter is arranged on inlet pipe to measure rate of flow. Compressed air is supplied to the fluidizing column so as to make sure that the bed gets fluidized. About 15 liters of effluent sample from a local bio-diesel industry (Atchutapuram, Visakhapatnam) is collected each day and diluted to 1:5 concentrations and is used as stock solution for experimentation. A concentrated biomass solution is prepared using tomato slurry mixed with the wet sludge collected from domestic sewage plant, in aerobic conditions. The process is continued for a week and the slurry obtained at the end is introduced into the experimental columns to act as seed for biomass acclimatization on bed particles in the columns.

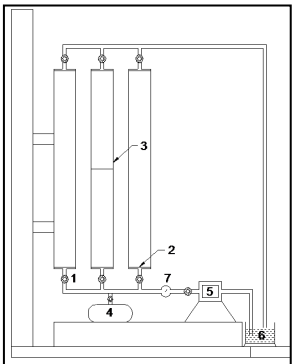

1. Vlave 2.Stainless Steel Mesh
3. Acrylic Glass Columns 120 cm long
4.Air Compressor 5. 0.5 HP Motor
6. Stock Solution 7.Flow meter

Fig.1 Experimental Setup

III. Methodology

The acclimatized biomass is transferred to the experimental columns and the columns are filled with water for three days before the start of experiment, and then the experiment is carried out by pumping the effluent taken from the local bio-diesel industry. The initial values of BOD and COD are determined. The samples from outlet of the experimental columns are collected at intervals of 30min, 60min, 90 min and the respective BOD and COD values are determined. The same experiment is carried out with different bed materials. The process is continued till the constant percentage removals of BOD and COD are obtained.

The reaction rate coefficients are determined using the experimental results obtained using the method of integration which involves the substitution of the measured data of the amount of reactant remaining at various times into the integrated form of the rate expression. Zero, First and Second order reaction expressions are used to find the Reaction rate coefficients. The microbial decay coefficients are calculated using the specific substrate utilization rate (U) and the specific growth rate (μ).

IV. Results and Discussions

The percentage removals of BOD and COD at different operation times using MBBR Media (Plastic), Pumice Stones and Foam Pieces as bed materials are as shown in Fig 2 to 7.

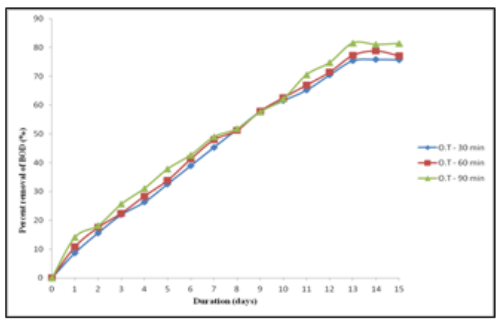

Fig.2 Percentage removal of BOD using MBBR Media(Plastic)

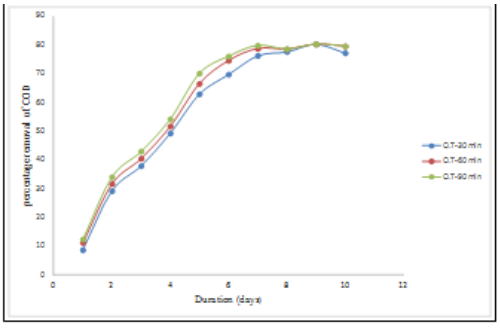

Fig.5 Percentage removal of COD using MBBR Media(Plastic)

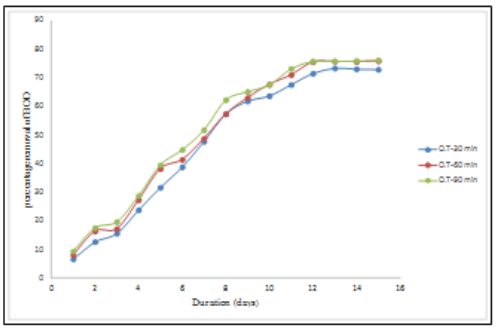

Fig.3 Percentage removal of BOD using Pumice Stones

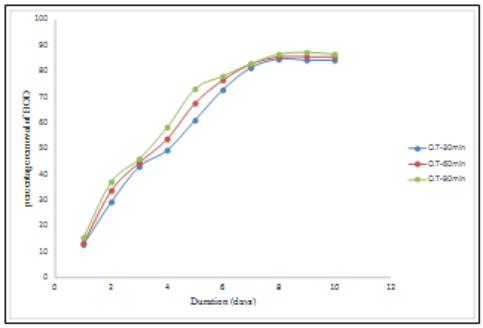

Fig.6 Percentage removal of COD using Pumice stones

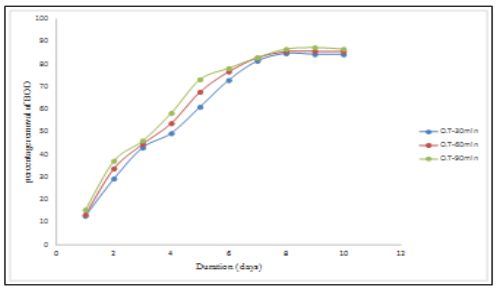

Fig.4 Percentage removal of BOD using Foam Pieces

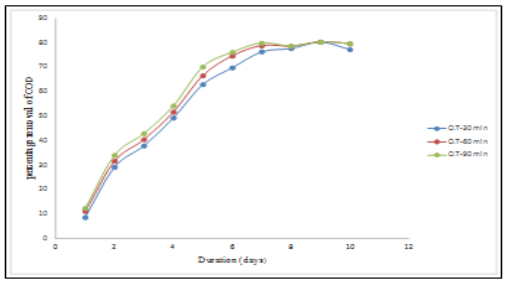

Fig.7 Percentage removal of COD using Foam Pieces

It is observed that the maximum percentage removal for BOD is found to be 87.39%, 83.32%,76.38%, for the bed materials Foam pieces, Commercially available MBBR media(Plastic), Pumice stones respectively, at an operation time of 90 minutes. Similarly the maximum percentage removals of COD are found to be 80.39%, 73.32%, 65.38%, respectively, for the bed materials in the same order respectively. The experimental duration/the acclimatization period is found to be 10, 14, and 15 days against the bed materials Foam pieces, Commercially available MBBR media (Plastic), Pumice stones respectively. From these results it is observed that, Foam is found to be a good alternative for the Commercially available MBBR (plastic) media.

V. Reaction Rate and Microbial Growth Coefficients

For the study on Reaction Rate Coefficients, three different reaction rate models are taken into consideration viz., Zero order, First order and Second order reaction. Plots of the integrated forms of the reaction rate expressions are used to determine the reaction rate coefficients 'k'. The experimental programme conforms to first order reaction rate kinetics. The first order reaction rate coefficients (k) obtained for the experiments with three different bed materials ranged from 0.07day^{-1} to 0.23day^{-1} at different operation times. First order kinetics for the removal of BOD and COD for the three bed materials at the operation time of 90 min are shown in Fig 8 to 13. These are in agreement with the earlier experimental works [5, 6, 7] referred. At the same time, these coefficients are found to be more for the experiment with Foam Pieces as bed material.

The microbial decay coefficients (k_d) are obtained using the specific growth rates (μ) and specific substrate utilization rates (U), as presented in Table 1. It is observed that, the microbial decay coefficient (k_d) are found to be increasing against the following order of usage of bed materials. i.e., Pumice stones, MBBR media (plastic), and Foam Pieces for different operation times and at the end of the acclimatization period. Maximum microbial decay coefficient 'k_d' values are obtained when Foam Pieces are used as bed material when compared to Pumice stones and MBBR media (plastic). The Microbial decay coefficients obtained in the study are well in agreement with earlier works [8,9].

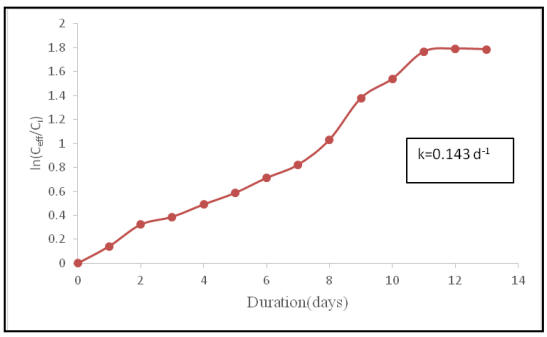

Fig.8 First order kinetics for the removal of BOD (Bed material: MBBR media)

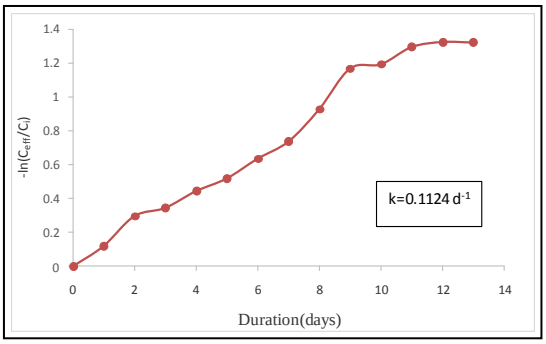

Fig.11 First order kinetics for the removal of COD (Bed material: MBBR media)

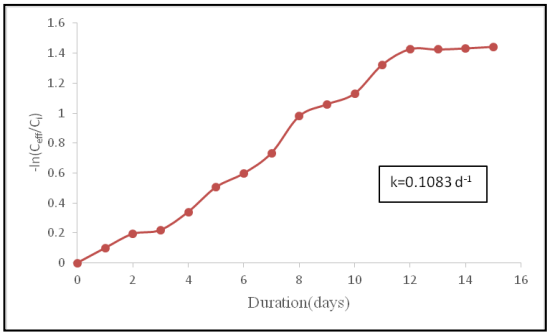

Fig.9 First order kinetics for the removal of BOD (Bed material: Pumice Stones)

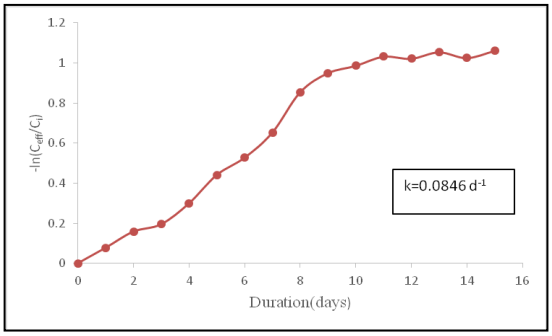

Fig.12 First order kinetics for the removal of COD (Bed material: Pumice Stones)

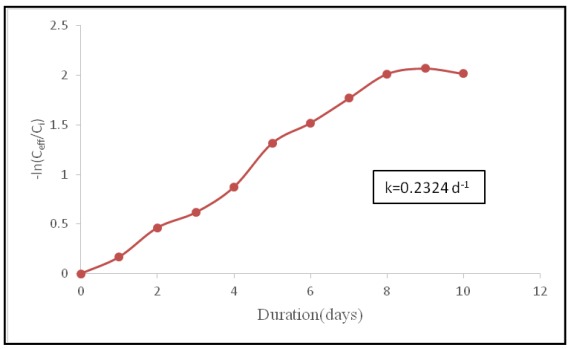

Fig.10 First order kinetics for the removal of BOD (Bed material: Foam pieces)

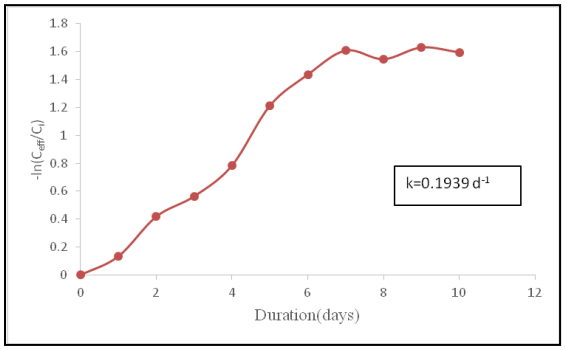

Fig.13 First order kinetics for the removal of COD (Bed material: Foam pieces).

Table 1 The Microbial Decay Coefficients (k_d)

S.No	Bed material	Operation time (minutes)	Microbial Decay Coefficient (kd), day-1 For BOD
1	Bio carriers (Plastic)	30	0.003
		60	0.0034
		90	0.0037
2	Pumice stones	30	0.003
		60	0.002
		90	0.003
3	Foam	30	0.005
		60	0.004
		90	0.004

VI. Conclusions

1) The FBBR has acclimatized in 10, 14 and 15 days against the usage of bed material viz., Foam pieces, Commercially available MBBR media(Plastic), Pumice stones respectively.
2) The maximum percent removal of BOD and COD are found to be more in the experiments conducted with Foam Pieces as bed material.
3) The reaction rate kinetics of the experimental programme conform to first order reaction rate kinetics and the reaction rate coefficients (k) obtained are in agreement with the earlier works.
4) The microbial decay coefficient (k_d) are found to be increasing against the following order of bed materials. i.e., Pumice stones, MBBR media (plastic) and Foam Pieces for different operation times and at the end of the acclimatization period.
5) Therefore, it can be concluded that, Foam Pieces can be used as a better alternative against the Commercially available MBBR media (plastic) for the removal of both BOD and COD in FBBRs.

References

[1] C. Nicolella a'1, M.C.M. van Loosdrecht b, J.J. Heijnen, Wastewater treatment with particulate biofilm reactors - Journal of Biotechnology 80 (2000) page,1-33,Netherlands.

[2] G.V.R.Srinivasa Rao, K.Srinivasa Murthy, P.Chaitanya Kumar, A Study on the removal of cod using laboratory scale Fluidized bed Bioreactors, IJERD, Vol 7, Issue 3, P. 33-37; 2012

[3] Qasim S (1999) Wastewater treatment Plants, Planning,Design and Operation,2nd ed., Technomic Publishing Co., Lancaster,PA.

[4] Metcalf & Eddy, 1991. Wastewater Engineering - Treatment Disposal Reuse - 3rd Edition, McGraw-Hill

[5] Adebayo G. B, Jimoh A. A., Odebunmi E.O and Oke M. A, Kinetics study of bioremediation of industrial effluents by Pseudomonas spp and Bacilluss using chemical oxygen demand (COD) Research Journal of Agriculture and Environmental Management. Vol. 2(9), September, 2013, 261-269, Nigeria

[6] G. Nakhla,, Victor Liu b , A. Bassi, a Kinetic modeling of aerobic biodegradation of high oil and grease rendering wastewater, Bioresource Technology 97 (2006) 131–139, Canada.

[7] Hamza U D, Mohammed I A and Ibrahim S, Kinetics of Biological Reduction of Chemical Oxygen Demand from Petroleum Refinery Wastewater- Researcher, 1(2), 2009 page 17-23, Nigeria

[8] Rangasamy Parthiban Biodegradation kinetics during different start up of the anaerobic tapered fluidized bed reactor - Songklanakarin J. Sci. Technol. 33 (5), 539-544, Sep. - Oct. 2011,India

[9] R.R.Souza, I.T.L.Bersolin, T.L.Biono, M.L. Gimenesnd,B.P.Dias- Filho ,The performance of a Three- Phase Fluidized bed reactor in Treatment of Wastewater with High Organic Load, Brazilian Journal of Chemical Engineering; 21(2),page 219-227; 2004,Brazil

ISSN (e): 2250 – 3005 || Volume, 05 || Issue, 08 ||August – 2015 ||
International Journal of Computational Engineering Research (IJCER)

Studying & Evaluating the Performance of Solar Box Cookers (Untracked)

Mohammed Hadi Ali
Assistance Professor, University of Mustansiriya

Abstract

The primary aim of this study was to conduct the performance evaluation on solar cooker design. The secondary aim was to build and developing of a new and efficient solar cooker design. A direct solar box cooker (Untracked type) was tested in this study with low cost feature and low technology. The testing for the solar box cooker was conducted at the top roof of Material Engineering Department building. In this test, three water quantities (1.5, 1 and 0.5 kg) were used in order to find the effect of the mass quantity of cooking food on the temperature rise inside the solar cooker. The results showed that the attainable temperature reached a maximum cooking temperature of (81.6 ^{o}C) for water mass quantity of (1000 grams) with temperature difference between the cooking temperature and the ambient temperature of (61.5 ^{o}C). But a lower maximum temperature (81.7 ^{o}C) for (500 grams) the reason for that is due the lower solar intensity during the test of partially cloudy day. As a conclusion, it was found that as the solar intensity increases the cooking temperature increases too. The other factor which influences the cooking temperature is the cooking mass as the cooking mass increases the cooking temperature decreases. Although the cooking temperature increases but the standardized Power decreases, this is because the increasing in cooking temperature is not equalizing or go in parallel with the decreasing in cooking mass, thus it is preferable to use solar cooker for adequate cooking mass quantity to get a high merit or advantage solar cookers.

I. Introduction

The increasing demand of electricity, the exhaustion of wood/charcoal consumption and the rapid inflating of fuel price, the environmental degradation, have lead countries to encourage the use of renewable energy [1], one of this renewable energy is the solar energy. There is a long history for humans to use solar energy. They used steel mirror to concentrate the sunlight for inflaming a fire, and they used solar energy for drying agriculture crop. In recent times, the use of solar energy is widely spread; including solar thermal usage, solar photovoltaic employment and solar photochemical application etc., solar power is simply can be said as the of sunlight conversion into electricity [2]. In many developing countries especially in rural area, they can play a major role in developing good living situations among low-income families by lowering and reducing fuel resources. However, many rural areas do not have an electricity grid net, in order that people can access to and use electricity as a fuel source. Additionally, other fuels such as gas net can be difficult to connect between the towns and rural area due to the large distances and inadequate road networks. These reasons give the people to justify their using and deployment of solar cookers and necessitate research into their operation [3].

Solar cooking presents an alternative energy source for cooking. It is a simple, safe and convenient way to cook food without consuming fuels, heating up the kitchen and polluting the environment. It is appropriate for hundreds of millions of people around the world with scarce fuel and financial resource to pay for cooking fuel. Solar cookers can also be used for boiling of drinking water, providing access to safe drinking water to millions of people thus preventing waterborne illnesses. Solar cookers have many advantages, on the health, time and income of the users and on the environment. In tropical countries, the solar energy is plenty and therefore it becomes a reliable and sustainable source of energy [4].

This paper presents a model of untracked solar box cooker with four side reflectors using solar energy for cooking has been designed, fabricated and experimentally studied to produce heat from solar energy which is used to reduce the consumption of electricity or conventional fuel where it is difficult to supply to rural and desert areas.

II. The Research Goal

The goal of this paper is to carry out a design, fabrication, investigation and testing the model of an untracked solar box cooker prepared for this study to obtain the thermal performance for such type and taking into account all the points to gain heat and reducing the heat losses.

III. Experimental Rig Description

The solar cooker model is made mainly of plywood with an overall dimensions (40 cm X 40 cm X 40 cm), it consist of the following parts [figure (1)]:

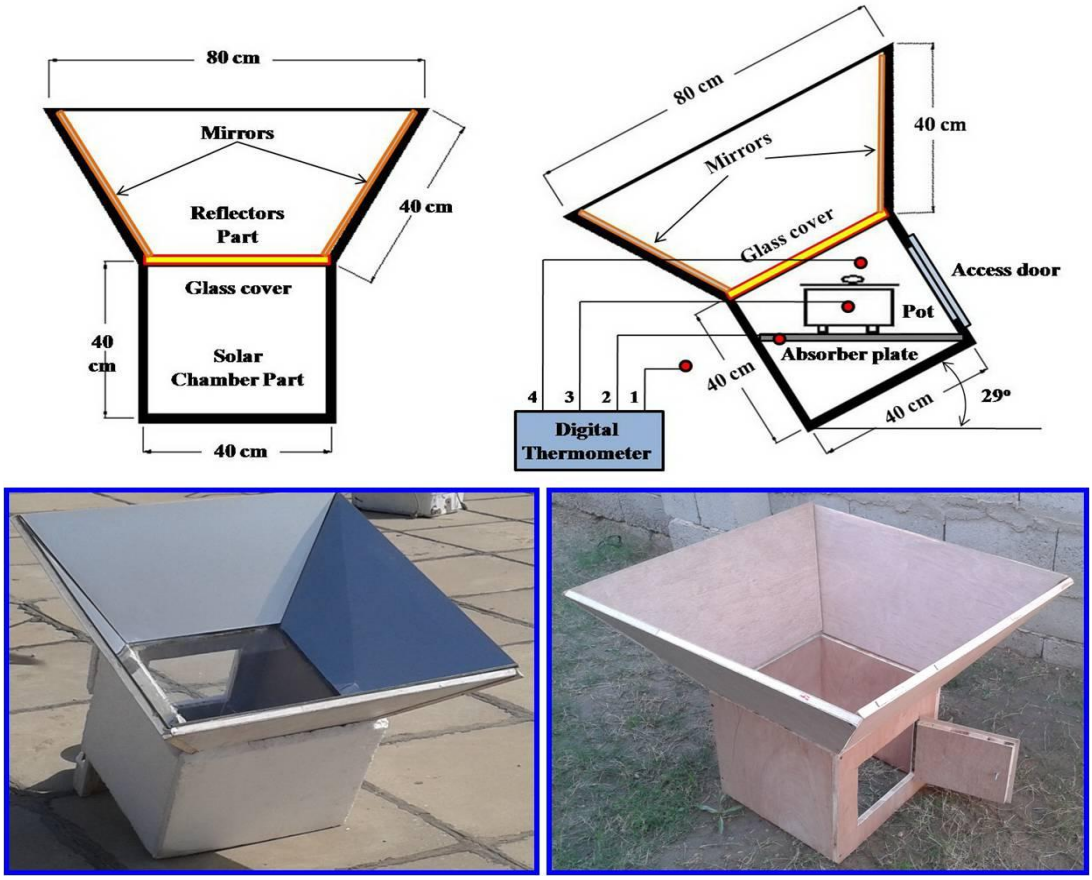

Figure (1): the solar box cooker with four sides reflectors prototype.

1. The aperture window of [40 cm X 40 cm] made of glass cover (6 mm thickness) which is supported by cooker sides' structure, the purpose of the glass cover is to close the solar box and help to capture and trap the solar heat inside the solar box.
2. A dark absorber plate exposed to solar radiation aligned horizontally inside the cooker chamber is made of a thick aluminum plate of (3 mm) thickness, to highly absorbing the solar heat incident on it.
3. The four reflectors [trapezoidal shape of lower base of (40 cm), upper base of (80cm) and height of (40 cm)] were covered with mirrors which are well stuck to reflectors using special glue. The reflector angles for the solar cooker were tilted with (30^0) with the vertical showing the best amount of admitted sunlight can captured into solar cooker [5]. The mirrors were used to reflect and direct the solar rays into the solar oven through the glass cover.
4. The cooker sides and its bottom were insulated with a Polystyrene board of (50 mm) thickness. This will help to reduce the heat dissipated outside the cooker and to improve its performance, the only side to loss heat form the solar cooker is from the glass cover which is exposed to the sky.
5. The solar cooker was oriented according to Baghdad latitude which is (33.4^o degree) in the northern sector of earth. The tilt angle was calculated for Baghdad city to be found equal to (29^o degree) by using the following formula [6] for latitude between (25^o to 50^o):

$$tilte\ angle = (latitude * 0.76) + 3.1^o$$

6. A pot with cover made of aluminum is used to warm (cooking) water inside it. The pot is painted with black color in order to highly absorbing the solar heat incident on it, it will get warm faster.
7. The measuring instruments used in this experiment include the digital thermometer instrument and digital solar intensity instrument:

- Two digital thermometers model (TM – 924C) each of two channels thermocouple are connected in order to measure temperature in four positions:
  T_1 : is the ambient temperature outside the solar cooker (°C) .
  T_2 : is the temperature of the absorber plate (°C).
  T_3 : is the temperature of the cooking water inside the pot (°C).
  T_4 : is the temperature inside solar cooker chamber (°C).

For measuring these four temperatures, it was used a special thermocouple type (K) in which it is connected to the dual thermometer instrument.

- The digital solar radiation instrument is used to measure the horizontal solar intensity [model solar power measuring instrument type (SPM – 1116 SD), which is applicable to measure the solar radiation and solar power.
- The wind speed (V) was determined using the digital Thermo – Anemometer (model: AM-4210E).

IV. Theoretical Analysis

In this paragraph, and in order to determine the performance of the solar cooker prototype, the standard which was originally developed by Dr. Paul Funk as an international testing standard for solar cookers was used. This standard was recognized at the Third World Conference on Solar Cooking, in January of 1997 (Funk, 2000). The goal of this standard was to produce a simple, yet meaningful and objective measure of cooker performance that was not so complicated as to make testing in less developed areas prohibitive.

Temperature measurements are made of the water and averaged over 10 minute intervals. Ambient temperature and normal irradiance (solar energy flux per area) are also measured and recorded. This is calculated through the following procedure [7]:

$$P = \left(\frac{T_2 - T_1}{600}\right) * m * C_p \quad \ldots (1)$$

Where:

P = cooking power (W)
T_2 = final water temperature (^oC)
T_1 = initial water temperature (^oC)
m = mass of water (kg)
C_p = heat capacity (4168 J/kg. K)

Equation (1) was divided by (600 sec.) of each (10 minute) to get the power produced by the solar cooker in each (10 minute).

To determine the standardized cooking power (P_s), (P) is multiplied by the standard and normalized solar irradiance figure of (700 W/m^2) and divided by the average global irradiance of that interval through the following equation:

$$P_s = P\left(\frac{700}{I}\right) \quad \ldots (2)$$

Where:

P = cooking power (W)
P_s = the standardized cooking power (W)
I = interval average insolation (W/m^2)

Tests were performed to study and evaluate the performance for Solar Cookers (Un-Tracked) and Reporting Performance according to (Funk, 1997), with and under the following conditions [8]:

• Testing was carried out between 9:00 and 14:00 solar time.
• Ambient temperature and wind speed were recorded (it is less than 2.5 m/s).
• The test began with water at ambient temperature. Cooking temperature was recorded.
• The horizontal irradiance were recorded and averaged for a 10- minute interval.
• Wind speeds greater than (2.5 m/s) and ambient temperatures below (20 ºC) were disregarded.

V. Results and Discussion

In this paragraph, the analysis for this research shows the possibility to evaluate the solar cooker performance by using three different quantities of water as a cooking food. Those quantities are (1.5 kg, 1 kg and 0.5 kg); in this way the standardized cooking power (P_s) can be predicted and used as a factor of merit to show the solar cooker performance.

The testing was carried out at three successive days from (19 to 21April). The measured temperatures for the water mass for (1.5 kg), the absorber plate, the solar cooker chamber temperature and the ambient temperature,

Figure (2) showing the temperatures variation with solar time conducted between (9:00 morning and 14:00 afternoon).

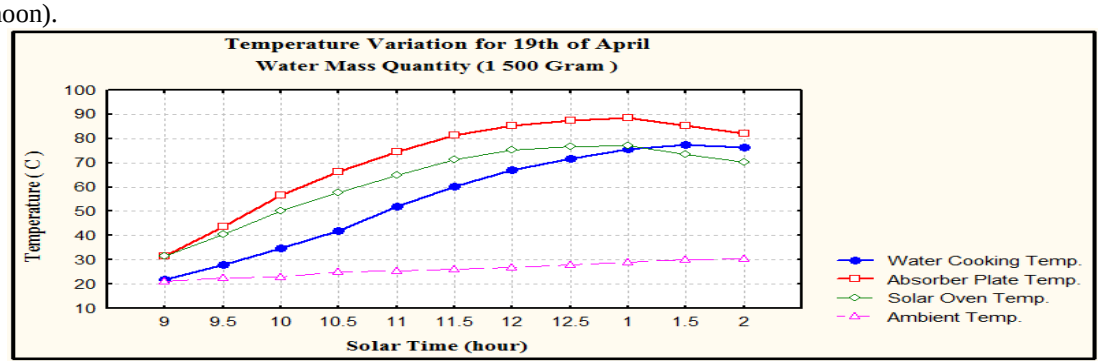

Figure (2): The temperatures variation for (1.5 kg) water mass.

The water cooking temperature is risen at the beginning of heating to a maximum temperature of (76.6 ^{o}C) at solar time of (1:30 afternoon) and start to fall down, while the absorber plate temperature reaches its maximum temperature of (88.6 ^{o}C) at (1:00 afternoon) and the solar cooker's chamber temperature has its maximum temperature of (77.2 ^{o}C) at (1:00 afternoon). The maximum temperature difference between the water cooking temperature and the initial water temperature is at (1:30 afternoon) is (56.7 ^{o}C).

In the same manner, **figure (3)** showing the temperatures variation with solar time conducted between (9:00 morning and 14:00 afternoon) for water mass of (1 kg). The maximum water cooking temperature of (82.3^{o}C) at solar time of (1:30 afternoon) was obtained, while the absorber plate temperature reaches its maximum temperature of (96.1^{o}C) at (12:00 afternoon) and the solar cooker's ambient temperature has its maximum temperature of (84 ^{o}C) at (12:00 afternoon). The maximum temperature difference between the water cooking temperature and ambient temperature is at (1:30 afternoon) is (62.2 ^{o}C).

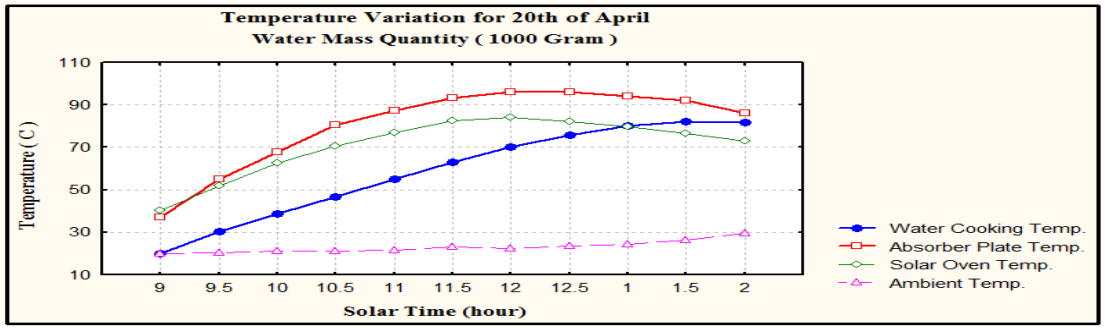

Figure (3): The temperatures variation for (1 kg) water mass.

In the same manner, **figure (4)** showing the temperatures variation with solar time conducted between (9:00 morning and 14:00 afternoon) for water mass of (0.5 kg). The maximum water cooking temperature of (83 ^{o}C) at solar time of (1:30 afternoon) was obtained, while the absorber plate temperature reaches its maximum temperature of (93.2 ^{o}C) at (12:30 afternoon) and the solar cooker's ambient temperature has its maximum temperature of (82.3 ^{o}C) at (12:30 afternoon).

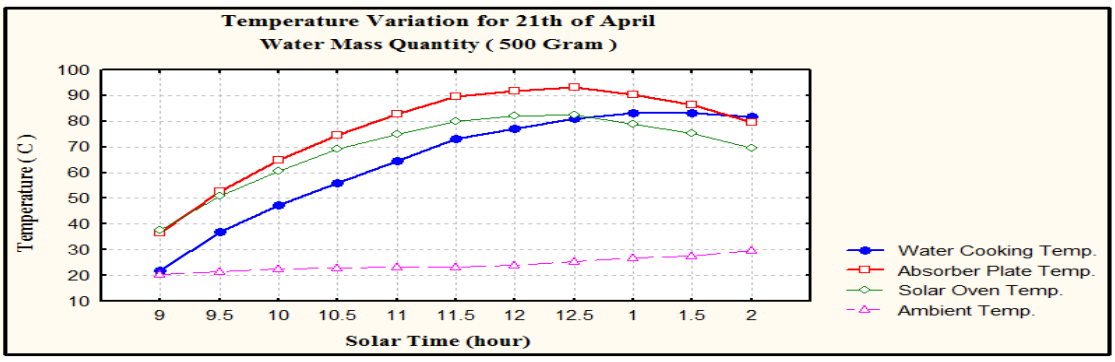

Figure (4): The temperatures variation for (0.5 kg) water mass.

The maximum temperature difference between the water cooking temperature and ambient temperature is at (1:30 afternoon) is (62.5 ^{o}C).

Figures (5, 6 and 7) showing the water cooking temperatures and solar intensity falling on the solar cooker against solar time. It was noticed that at the beginning the water cooking temperature increases due the solar heat accumulated inside the solar oven and trapped inside the solar oven, then it will begin to fall down as the solar radiation intensity decreases at solar time of (12:00 noon).

The highest water cooking temperature that is being obtained is (83.2 ^{o}C) for water mass quantity of (0.5 kg) on (21st of April) which a dusty day (not clear and shine), it could be reached to higher temperature but it can be concluded from the figure (7) that the solar intensity less than the other measuring days (19th and 20th of April) as a result less average total solar radiation incident on the solar oven and thus a lower maximum water cooking temperature was obtained.

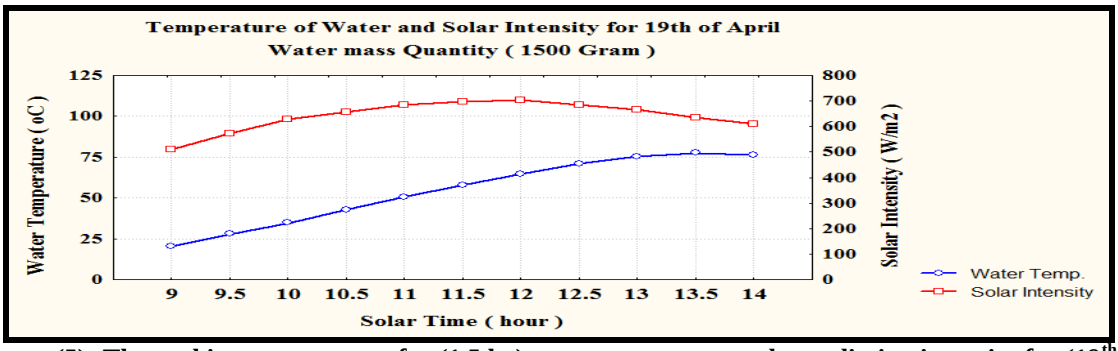

Figure (5): The cooking temperature for (1.5 kg) water mass versus solar radiation intensity for (19th of April).

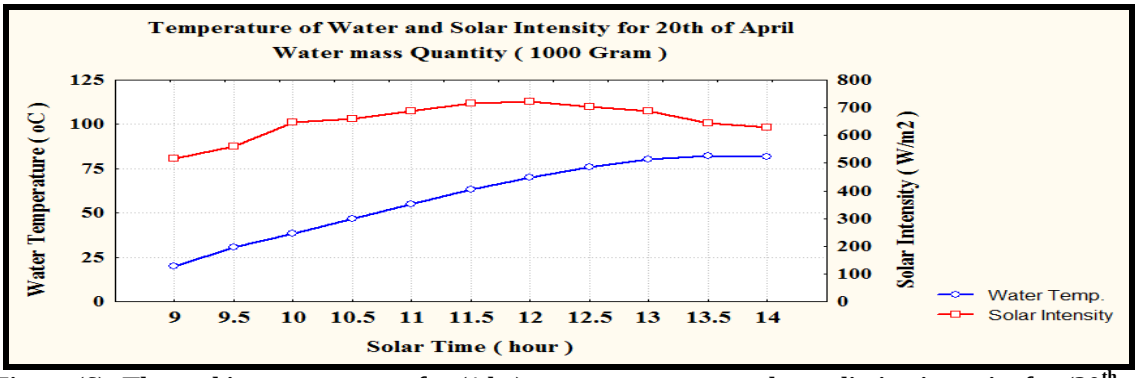

Figure (6): The cooking temperature for (1 kg) water mass versus solar radiation intensity for (20th of April).

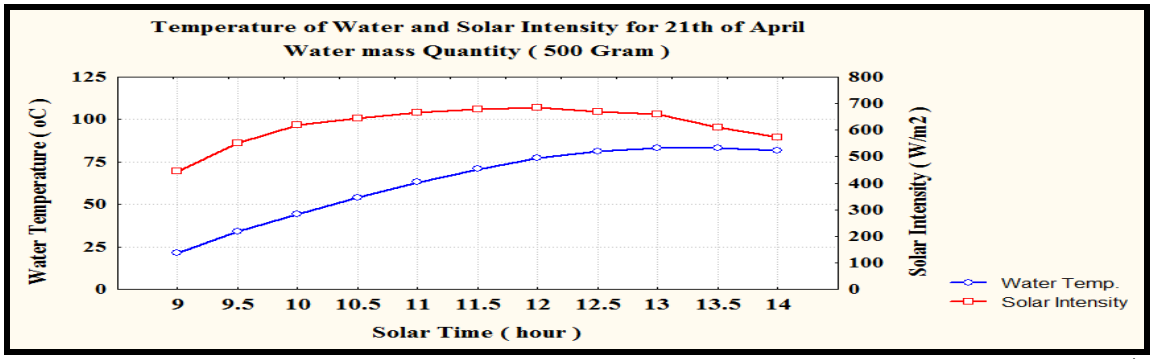

Figure (7): The cooking temperature for (0.5 kg) water mass versus solar radiation intensity for (21stof April).

As a conclusion, the cooking temperature increases as the average solar radiation intensity increases and vice versa during the conducted solar time interval that will be used for cooking.

Another point that affects the temperature rise of cooking water is the mass quantity which is used in cooking, and as the mass quantity which is used in cooking increases yielding to a lower cooking temperature.

Figures (8, 9 and 10) showing the performance of the solar box cooker (Standardized Cooking Power) which has been established versus the temperature differences. It was noticed that the performance for solar box cooker increases as the temperature difference increases too, but the most important point is as the water quantity increases the performance for solar box cooker increases too.

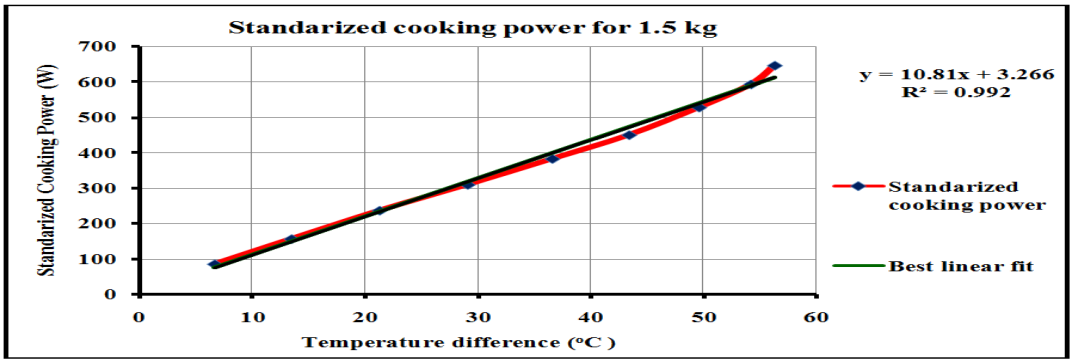

Figure (8): The Standardized Cooking Power for (1.5 kg) water mass versus temperature difference between Pot content at initial and final temperature.

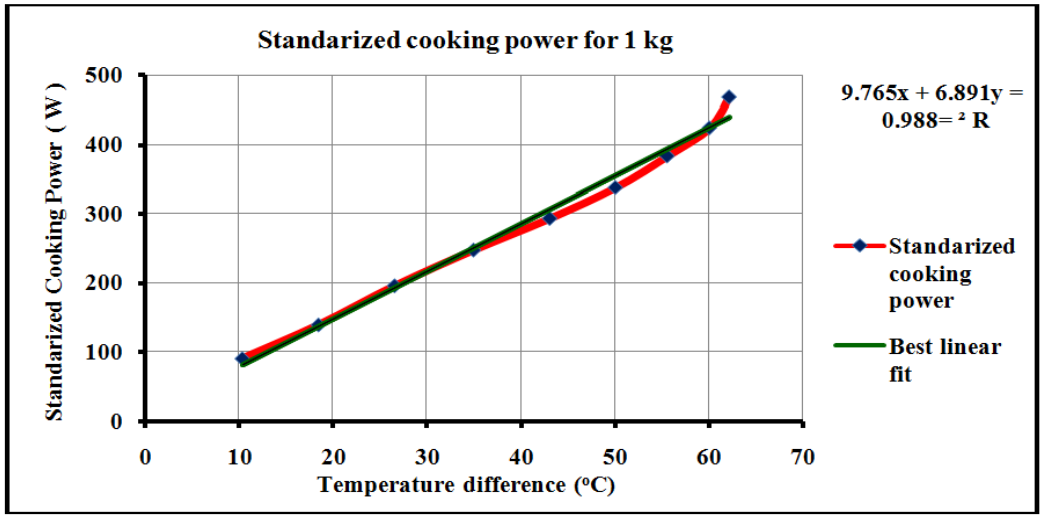

Figure (9): The Standardized Cooking Power for (1 kg) water mass versus temperature difference between Pot content at initial and final temperature.

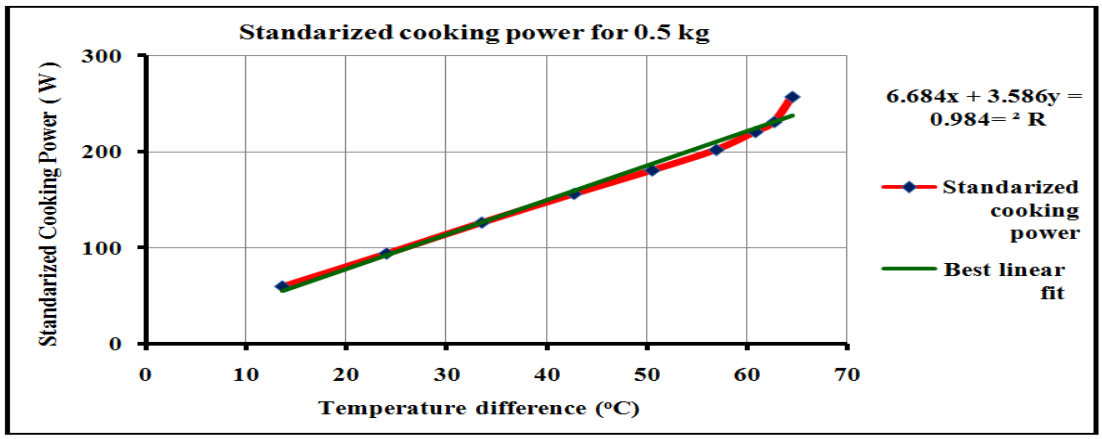

Figure (10): The Standardized Cooking Power for (0.5 kg) water mass versus temperature difference between Pot content at initial and final temperature.

The highest standardized cooking power was obtained for water quantity of (1.5 kg) which was reached to about (650 W), while the lowest was obtained for (0.5 kg) which was reached to about (270 W).

This is because the increasing in cooking temperature is not equalizing or go in parallel with the decreasing in cooking mass, thus it is preferable to use solar cooker for adequate cooking mass quantity to get a high merit or advantage solar cookers.

Figures (8, 9 and 10) showing too, the best linear fitting curve equations for the different water quantities and its coefficient of fitness (R^2). The coefficients of fitness for them is not less than (0.98)

References

[1] Chaouki Ali, *et. al*., 2010, "Theoretical Study and Design of a Hybrid Solar Cooker**",** IJRRAS, Volume (3), Issue (3), 2010.

[2] A. Claude *et al*., 2012, "Engineering, design and fabrication of a solar cooker with parabolic concentrator for heating, drying and cooking purposes", Archives of Applied Science Research, Vol. (4), Issue (4), 2012.

[3] R.Gayapershad, S.T. Dladla and M.J. Brooks, "Preliminary Results from a Performance Evaluation Study of Commercial Solar Cookers", http://www.wcpsd.org/posters/environment/Gayapershad.pdf

[4] C Z M Kimambo, 2007, "Development and performance testing of solar cookers", Journal of Energy in Southern Africa • Vol 18 No 3 • August 2007.

[5] Dean Still and Jim Kness, "Heat Capturing, Five Earth-Friendly Cooking Technologies & How to Build Them", Aprovecho Research Center, Mexico.

[6] Charles R. Landau, "Optimum Tilt of Solar Panels", 2014, http://www.solarpaneltilt.com/[10/31/2014 10:38:53 PM]

[7] Shawn Shaw, "Development of a Comparative Framework for Evaluating the Performance of Solar Cooking Devices", http://images3.wikia.nocookie.net/__cb20080215190132/solarcooking/images/e/e5/Shawn_Shaw_thesis_on_solar_cooker_testing_standards.pdf

[8] R.Gayapershad, S.T. Dladla and M.J. Brooks, " Preliminary Results from a Performance Evaluation Study of Commercial Solar Cookers", http://www.wcpsd.org/posters/environment/Gayapershad.pdf

ISSN (e): 2250 – 3005 || Volume, 05 || Issue, 08 ||August – 2015 ||
International Journal of Computational Engineering Research (IJCER)

Frequency Identification Approach For Wiener Systems

Adil Brouri, Smail Slassi
ENSAM, Université Moulay Ismail, L2MC, AEEE Depart, Meknes, Morocco

Abstract:
Wiener systems identification is studied in presence of possibly infinite-order linear dynamics and static nonlinearity. The problem of identifying Wiener models is addressed in the presence of hard nonlinearity. This latter is not required to be invertible of arbitrary-shape. Moreover, the prior knowledge of the nonlinearity type, being e.g. saturation effect, dead zone or preload, is not required. Using sine excitations, and getting benefit from model plurality, the identification problem is presently dealt with by developing a two-stage frequency identification method.

Keywords: *Wiener model, Hard nonlinearity, frequency identification.*

1. Introduction

The Wiener model is a series connection of a linear dynamic bloc and a memoryless nonlinearity (Fig. 1). When both parts are parametric, the identification problem has been dealt with using stochastic methods (e.g. Wigren, 1993, 1994; Wills and Ljung, 2010; Vanbeylen et al., 2009; Vanbeylen and Pintelon, 2010) as well as deterministic methods (e.g. Vörös, 1997, 2010; Bruls et al., 1999). The stochastic methods enjoy local or global convergence properties under various assumptions e.g. the system inputs should be persistently exciting (PE) or Gaussian and the system nonlinearity is invertible. The last limitation has recently been overcome by Wills et al. (2011). Multi-stage methods, involving two or several stages, have been proposed in (e.g. Westwick and Verhaegen, 1996; Lovera et al., 2000) and their consistency was ensured if the inputs are Gaussian and the nonlinearity is odd. Deterministic parameter identification methods consist in reformulating the problem as an optimization task, generally coped with using various relaxation techniques. Then, local convergence properties ensured in presence of PE inputs. Nonparametric Wiener systems (where none of the linear subsystem or the nonlinear element assumes a priori known structure) have been dealt with using both stochastic and frequency methods. In the stochastic methods (e.g. Greblicki and Pawlak, 2008; Mzyk, 2010), the nonlinearity is generally determined using variants of the kernel regression estimation technique while the (unknown) coefficients of a FIR/IIR approximation of the linear part are estimated using cross-correlation analysis. Several assumptions are needed e.g. Gaussian inputs, FIR linear dynamics, Lipschitzian nonlinearity. In frequency methods, the linear subsystem frequency response and the nonlinearity map are determined in two or several stages (e.g. Giri et al., 2013, 2014; Brouri et al., 2014).

In this paper, the problem of identifying Winer systems is addressed, for simplicity, in the continuous-time. Unlike many previous works, the model structure of the linear subsystem is entirely unknown. Furthermore, the system nonlinearity is of hard (Figs. 2a-b) type and is not required to be invertible.

The present strategy is allowed to interest a wide range of the system nonlinearity (Figs. 2a-b). The identification problem amounts to determining an accurate estimate of the (nonparametric) frequency response $G(j\omega)$, for a set of frequencies $(\omega_1 \dots \omega_m)$, and the nonlinearity. The present identification method is a two-stage: the system nonlinearity is identified first, using simple constant inputs, and based upon in the second stage to identify the linear subsystem.

The paper is organized as follows: the identification problem is formulated in Section 2; the nonlinear operator identification is coped with in Section 3; the linear subsystem frequency response determination is investigated in Section 4; simulation results are presented in Section 6.

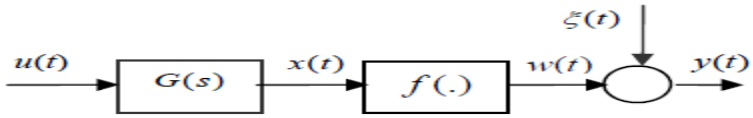

Fig. 1. Wiener model with hard nonlinearity $f(.)$

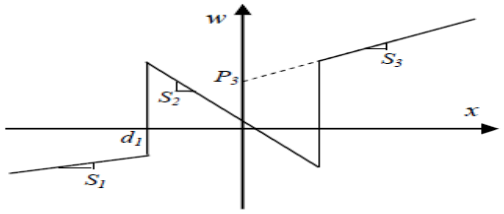

Fig. 2a. Nonlinearity hard

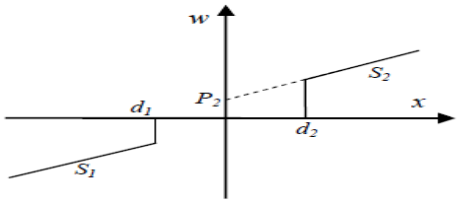

Fig. 2b. Nonlinearity hard with preload and dead zone

2. Identification of system nonlinearity

Standard Wiener systems consist of a linear dynamic subsystem $G(s)$ followed in series by a memoryless nonlinear operator $f(.)$ (Fig. 1). More specifically, the Wiener system under study is analytically described by the following equations:

$$x(t) = g(t) * u(t) \quad \text{with} \quad g(t) = \mathrm{L}^{-1}(G(s)) \quad (1)$$

$$y(t) = w(t) + \xi(t) \quad \text{with} \quad w(t) = f(x(t)) \quad (2)$$

where $u(t)$ and $y(t)$ denote the control input and the measured output; $x(t)$ and $w(t)$ are inner signals not accessible to measurement. The extra input $\xi(t)$ accounts for measurement noise and other modeling effects. It is supposed to be zero-mean ergodic and uncorrelated with the control input $u(t)$. The symbol * in (1) refers to the convolution operator and L^{-1} to the Laplace transform-inverse.

Accordingly, $g(t)$ denotes the impulse response of the linear subsystem and $G(s)$ its transfer function. It is just supposed that $g \in L_1$, so that the whole system becomes BIBO stable making possible open-loop system identification, with nonzero static gain (i.e. $G(0) \neq 0$). Interestingly, $G(s)$ is allowed to be infinite order. The system nonlinearity $f(.)$ is of hard (Figs. 2a-b) type and is not required to be invertible. Except for the above assumption $f(.)$ and $G(s)$ are arbitrary. In particular, the transfer function $G(s)$ is allowed to be non-parametric and of unknown structures. The static nonlinear element $f(.)$ may be noninvertible.

The problem complexity also lies in the fact that the non-accessible internal signals ($x(t)$, $w(t)$ and ξ) are not uniquely defined from an input-output viewpoint. In effect, if the couple $(G(s), f(x))$ is solution of the identification problem then, any model of the form $\left(\frac{G(s)}{K}, f(Kx)\right)$ is also solution of this problem whatever the real number $K \neq 0$. Therefore, without reducing the problem generality, one can assume $G(0) = 1$.

Accordingly, the system to be identified is described by the transfer functions:

$$\bar{G}(s) = \frac{G(s)}{G(0)} \quad (3)$$

and the nonlinearity:

$$\bar{f}(x(t)) = f(G(0)x(t)) \quad (4)$$

The modified system to be identified (i.e. $\bar{f}(.)$ and $\bar{G}(s)$) is the unique system satisfied the property: $\bar{G}(0) = 1$.

Then, the considered system is excited by simple constant inputs:

$$u(t) = U_j \quad \text{for} \quad j = 1 \ldots n \quad (5)$$

where the number n is arbitrarily chosen by the user, preferably sufficiently large. On the other hand, using the assumption of asymptotic stability of the linear subsystem and (3)-(5), the internal signal $x(t)$ is constant (i.e. $x(t) \xrightarrow[t\to\infty]{} X_j$). Then, one has, in the steady-state:

$$x(t) = U_j \quad \text{for} \quad j = 1 \dots n \tag{6}$$

Accordingly, it is readily seen, using (2), (4) and (6), that the undisturbed output is also constant, in the steady-state, i.e. $w(t) \underset{t\to\infty}{\to} W_j$. This latter can be expressed as:

$$W_j = \bar{f}(U_j) \quad \text{for} \quad j = 1 \dots n \tag{7}$$

Then, the system output is constant up to noise (in the steady-state). Finally, we can conclude using (7) that W_j (for $j = 1 \dots n$) only depends on the system nonlinearity $\bar{f}(.)$ and the input signal. Therefore, using the fact $\xi(t)$ is zero-mean, it follows from (2) and (7) that, the estimate of the steady-state undisturbed output W_j $(j = 1 \dots n)$ can be easily recovered using the following estimator:

$$\hat{W}_j(N) = \frac{1}{N}\sum_{k=1}^{N} y(k) \quad \text{for} \quad j = 1 \dots n \tag{8}$$

where N is any sufficiently large integer. Specifically, W_j can be recovered by averaging $y(t)$ on a sufficiently large interval. Then, a set of points $\left(U_j, \bar{f}(U_j)\right) = \left(U_j, W_j\right)$ (with $j = 1 \dots n$) belonging to nonlinearity $\bar{f}(.)$ can be determined. Finally, an accurate estimate $\hat{\bar{f}}_N(.)$ of $\bar{f}(.)$ can be easily obtained. These results lead to the following proposition:

Proposition 1. Consider the problem statement described by equations (1)-(2) and excited by the constant inputs (5). Then, one has:

1) $\hat{W}_j(N)$ converges in probability to W_j (as $N \to \infty$).
2) The nonlinearity $\hat{\bar{f}}_N(.)$ converges in probability to $\bar{f}(.)$ (as $N \to \infty$).

Proof. Part1. From the expressions (2) and (8) one easily gets:

$$\hat{W}_j(N) = \frac{1}{N}\sum_{k=1}^{N} W_j + \frac{1}{N}\sum_{k=1}^{N} \xi(k) = W_j + \frac{1}{N}\sum_{k=1}^{N} \xi(k) \quad \text{for} \quad j = 1 \dots n \tag{9}$$

Using the fact that, the noise signal $\{\xi(.)\}$ is zero-mean ergodic sequence, the last term in (9) converges to zero.
This establishes Part 1.
Part2. It readily follows from Part 1 and (7) that, the estimate points $\left(U_j, \hat{\bar{f}}_N(U_j)\right)$ converge to $\left(U_j, \bar{f}(U_j)\right)$ $(j = 1 \dots n)$. This completes the proof of Proposition 1.

3. Frequency gain identification

The aim of this subsection is to establish an estimator of the linear subsystem. The complex gain $G(j\omega)$ is characterized by the modulus gain $|G(j\omega)|$ and the phase $\varphi(\omega) = \angle G(j\omega) = \arg\left(G(j\omega)\right)$. The identification problem under study is dealt using a method based on the frequency approach. Firstly, by successively connecting the estimated points $\left\{\left(U_j, \hat{\bar{f}}_N(U_j)\right); j = 1 \cdots n\right\}$, a set of segments of $\bar{f}(.)$ is obtained (Figs. 2a-b). For reasons of identifiability, at least one segment must have a non-zero slope. Let q designates any segment have a non-zero slope. Then, the nonlinear system described in subsection 1 is excited with a given sine input:

$$u(t) = u_0 + U\sin(\omega t) \tag{10}$$

The choice of u_0 in (10) can be performed using the experimental data of nonlinearity estimator. It can take any value in the segment q. Accordingly, all resulting signals depend on the amplitude/frequency couple (U, ω). In steady state, these signals write:

$$x_{U,\omega}(t) = u_0 + U|G(j\omega)|\sin\left(\omega t + \varphi(\omega)\right) \tag{11a}$$

$$w_{U,\omega}(t) = f\left(x_{U,\omega}(t)\right) \tag{11b}$$

$$y_{U,\omega}(t) = w_{U,\omega}(t) + \xi(t) \tag{11c}$$

Note that, the signal $w_{U,\omega}(t)$ is periodic with period $2\pi/\omega$ and, accordingly, the working point $\left(x_{U,\omega}(t), w_{U,\omega}(t)\right)$ describes a closed cycle. Consequently, if $x(t)$ spans only the segment q, one gets:

$$w_{U,\omega}(t) = S_q\, x_{U,\omega}(t) + P_q \tag{12}$$

where $\left(S_q, P_q\right)$ is the couple parameters of segment q (Figs. 2a-b). S_q and P_q can be determined using the experimental data of nonlinearity estimator. If necessary, excite the system to be identified with other constant inputs U_j. Then, it readily follows from (11a) and (12):

$$w_{U,\omega}(t) = S_q\, U|G(j\omega)|\sin\left(\omega t + \varphi(\omega)\right) + P_q + S_q\, u_0 \tag{13}$$

Then, under these conditions, the undisturbed output $w_{U,\omega}(t)$ is a sine signal (in the steady state) with an offset $P_q + S_q\, u_0$. Furthermore, the curve $\left(U|G(j\omega)|\sin\left(\omega t + \varphi(\omega)\right), w_{U,\omega}(t)\right)$ is a straight line segment with slope $S_q\, U|G(j\omega)|$. If $S_q > 0$ (resp. $S_q < 0$), let $\bar{t}$ the first time, in the increasing (resp. in the decreasing) stages, satisfying:

$$w_{U,\omega}(\bar{t}) = P_q + S_q\, u_0 \tag{14a}$$

The expression (14a) implies:

$$S_q\, U\left|G(j\omega)\right|\sin\left(\omega\bar{t} + \varphi(\omega)\right) = 0 \tag{14b}$$

Then, one has the following relation between $\varphi(\omega)$ and $\bar{t}$:

$$\bar{t} = -\varphi(\omega)/\omega \quad \text{(modulo } 2\pi) \tag{15}$$

These results imply that, the complex frequency gains of the linear subsystem can be recovered if the undisturbed output $w_{U,\omega}(t)$ is accessible to measurement. At this stage, $w_{U,\omega}(t)$ is not measurable.

Fortunately, an accurate estimator of $w_{U,\omega}(t)$ exists, thanks to the (steady-state) periodicity of $w_{U,\omega}(t)$ and the ergodicity of the noise $\xi(t)$. The estimator, denoted $\hat{w}_{U,\omega,N}(t)$, is obtained by performing a T- periodic averaging with $T = 2\pi/\omega$ (Ljung, 1999, p. 232):

$$\hat{w}_{U,\omega,N}(t) = \frac{1}{N}\sum_{k=1}^{N} y_{U,\omega}(t + k\frac{2\pi}{\omega}) \quad \text{for} \quad t \in \left[0 \;\; \frac{2\pi}{\omega}\right) \tag{16a}$$

$$\hat{w}_{U,\omega,N}(t + k\frac{2\pi}{\omega}) = \hat{w}_{U,\omega,N}(t) \quad \text{for} \quad k = 1, 2, 3\ldots \tag{16b}$$

where N is any sufficiently large integer. The estimator (16a-b) is uniformly consistent i.e. $\hat{w}_{U,\omega,N}(t)$ converges (w.p.1 as $N \to \infty$) to $w_{U,\omega}(t)$, whatever t. Finally, it follows (14b) and (15) the gain modulus and the phase of the linear subsystem can be easily obtained using (16a-b).

4. Conclusions

The problem of system identification is addressed for Wiener systems where the linear subsystem, described by (1-2), may be parametric or not, finite order or not. The nonlinear element is of hard type. The latter are allowed to be noninvertible. The identification problem is dealt with using a two-stage approach combining frequency. Data acquisition in presence of constant inputs is performed in the first stage following the procedure of Section 2. Then, an accurate estimate of the system nonlinearity can be obtained. Data acquisition in presence of sine input excitations is performed in the first stage following the procedure of Table 1. Finally, the transfer function response is identified in the second stage using the algorithm described Section 3 and the estimator (16a-b). All involved estimators are consistent. To the author's knowledge no previous study has solved the identification problem for a so large class of Wiener systems

References

[1] T. Wigren. Recursive prediction error identification using the nonlinear Wiener model. Automatica, vol. 29, pp. 1011- 1025, 1993.
[2] T. Wigren. Convergence analysis of recursive identification algorithm based on the nonlinear Wiener model. IEEE Trans. Automatic Control, vol. 39, pp. 2191-2205, 1994.
[3] A. Wills and L. Ljung. Wiener system identification using the maximum likelihood method. In Giri F. & E.W. Bai (2010). Block-oriented nonlinear system identification. Springer, U.K, 2010.
[4] L. Vanbeylen, R. Pintelon, and J. Schoukens. Blind maximum-likelihood identification of wiener systems. IEEE Transactions on Signal Processing, vol. 57(8), pp. 3017–3029, 2009.
[5] L. Vanbeylen and R. Pintelon. Blind maximum-likelihood Identification of Wiener and Hammerstein nonlinear block structures. In Giri & Bai (eds), Block-Oriented Nonlinear System Identification, Springer, pp. 279-298, 2010.
[6] J. Vörös. Parameter identification of Wiener systems with discontinuous nonlinearities, Systems and Control Letters, vol. 44, pp. 363-372, 1997.
[7] J. Vörös. Compound operator decomposition and its application to Hammerstein and Wiener systems. In Giri & Bai, Block-Oriented Nonlinear System Identification, Springer, U.K, 2010.
[8] J. Bruls, C.T. Chou, B.R.J. Heverkamp and M. Verhaegen. Linear and nonlinear system identification using separable least squares, European Journal of Control, vol 5, pp.116-128, 1999.
[9] A. Wills, T.B. Schön, L. Ljung, B. Ninness. Blind Identification of Wiener Models. IFAC World Congress, Milan, Italy, 2011.
[10] D. Westwick and M. Verhaegen. Identifying MIMO Wiener systems using subspace model identification methods. Signal Processing, 52, pp. 235–258, 1996.
[11] M. Lovera, T. Gustafsson T., and M. Verhaegen. Recursive subspace identification of linear and non-linear Wiener statespace models. Automatica, vol. 36, pp.1639-1650, 2000.
[12] W. Greblicki, and M. Pawlak. Nonparametric System Identification. Cambridge University Press, 2008.
[13] G. Mzyk. Stochastic Identification of Wiener Systems. In Giri F. and E.W. Bai (2010). Block-oriented nonlinear system identification. Springer, U.K, 2010.
[14] F. Giri, A. Radouane, A. Brouri, F.Z. Chaoui. Combined frequency-prediction error identification approach for Wiener systems with backlash and backlash-inverse operators. Automatica, vol. 50, pp. 768-783, 2014.
[15] F. Giri, Y. Rochdi, A. Radouane, A. Brouri, F.Z. Chaoui. Frequency Identification of nonparametric Wiener systems containing backlash nonlinearities. Automatica, vol. 49, pp. 124-137, 2013.
[16] A. Brouri, O. Amdouri, F.Z. Chaoui, F. Giri. Frequency Identification of Hammerstein-Wiener Systems with Piecewise Affine Input Nonlinearity. 19th IFAC World Congress, Cape Town, South Africa, August 24-29, pp. 10030-10035, 2014.
[17] L. Ljung. System identification. Theory for the user. Prentice Hall, NJ, USA, 1999.

ISSN (e): 2250 – 3005 || Volume, 05 || Issue, 08 ||August – 2015 ||
International Journal of Computational Engineering Research (IJCER)

Determination of the Optimal Process Conditions for the Acid Activation of Ngwo Clay in the Bleaching Of Palm Oil

S .O Egbuna[1]., C. N Mbah [2]., T. O Chime[1].
[1]Department of Chemical Engineering, Enugu State University of Science and Technology, ESUT, Enugu.
[2]Department of Material and Metallurgical, Engineering, Enugu State University of Science and Technology, ESUT, Enugu.

ABSTRACT

In this work, the optimal adsorption parameters for the adsorption of Carotenoid in the bleaching of palm oil was investigated. Ngwo clay, a local adsorbent obtained from Ngwo town in the South-Eastern province of Nigeria, was used in the study. The palm oil used was also obtained from a local market in Enugu in the same region. The purpose of the work was to develop a model to optimize the efficiency of a local adsorbent that will be cheap and environmentally friendly, for the removal of pigments during refining of vegetable oils. The clay was first, acid activated and characterized, and used in the investigation. Central Composite Design (CCD) package was used to optimize the effects of process parameters of Temperature, Time and Clay Dosage on the bleaching efficiency of Palm Oil. A linear model was predicted and optimized based on BBD. This gave bleaching time of 40min., Temperature of 99.83^{o}C, and Clay dosage of 4%, at a predicted bleaching efficiency of 83%. The optimum conditions were validated to obtain an experimental value of 82.5% with 1.7% error condition.

Key words: *BBD, ANOVA, Ngwo Clay, Palm Oil , bleaching efficiency, Acid activation*

I. INTRODUCTION

Palm oil is one of the various types of vegetable oils belonging to the group called Lipids, because of its fatty acid content. [1] and [2], defined it as triglycerides extracted from plants. Most fats contain some colouring matters, either as a natural constituent, or as a discolouration produced during the processing, [2]. The natural pigments present in vegetable oils are mainly the caroteniods, giving yellow and red colours, and the chlorophylls, which give green colours, [3]. [4], observed that colour deterioration can also take place during the extraction process, especially in the local method of extraction used in most parts of the Eastern region of Nigeria. Removal, or reduction of colour and other pigmented components, otherwise called bleaching, according to ,[5], is necessarily, not only because a pale- coloured fat has an appeal of purity, [6], but also because the colours of the fat can influence the appearance of prepared food, and even more importantly, the pigment present may affect the flavour and stability of the fats and foods made from them. The decourloration (bleaching), could be achieved by chemical treatment, [7], by heat treatment, , [8], or by adsorption method, [9]; the most effective and widely used being the latter. Two methods are available for the refining of palm oil, namely, the physical and chemical methods. The refining operations, here include, degumming, neutratralization of free fatty acid, (FFA), for chemical process, using caustic soda, bleaching, to improve flavour and stability of the finished product, and deodorization to further reduce colour, and FFA, and improve stability. [10], noted that bleaching is the most important step in palm oil refining, especially in the physical process, since it is at this stage that most of the contaminants and oxidative products of Aldehydes and Ketones, are removed. [11] also observed that contact time, temperature, oil to adsorbent ratio, pressure, and other parameters, are the conditions that affect the performance of the bleaching process. Bleaching is done by using thermally activated clay, [12], or by acid activated clay, [13]. [14], said that the quality of raw material, (palm oil), is very important, since it relates directly to the processing cost, and product"s shelf life. [15], opined that colour and FFA content continue to fall with increasing bleaching earth, but the peroxide value is minimized after 30 minutes. They noted that the continuing fall in colour is attributed to the heat bleaching effect.

Bleaching temperature is one of the factors that affect the performance of the bleaching and degumming processes of raw palm oil. [10] have also observed that bleaching temperature has a great effect on the colour, FFA, PV and AV of oil being processed, and the keeping quality of the oil as shown in Figs. I and II, respectively. They noted that bleached oil colour tends to continuously fall as the temperature is increased, but

the deodorized oil colour reached a maximum when the bleaching temperature is about 100^{o}C. Oil – adsorbent ratio, is also of importance in determining the optimum performance condition of clay during bleaching, as it affects the efficiency of degumming and bleaching processes. The higher the clay dosage the more the colour reduction; the optimum clay dosage will however, depend on the quality and nature of the impurities in the raw palm oil [13]. [16] and [13], have developed the adsorption mechanism(model) for the adsorption of carotenoids on activated clay based on adsorption theory of Langmuir isotherm. [17], had earlier worked on the optimal bleaching performance of acid activated Ngwulangwu clay, using Central Composite Design (CCD) to optimize the process variables.

In this work,

- The optimal process conditions for palm oil bleaching was determined using Ngwo clay as an adsorbent
- BBD via Response Surface Method, was used to find the most suitable conditions to optimize the process variables
- The interaction between the variables was analyzed by applying the ANOVA method of analysis.

II. Materials and Methods

The clay and the oil used in the investigations were obtained locally from Ngwo Town, in Enugu, South East province of Nigeria. Tetraoxosulphate (VI) acid is used for the activation and petroleum ether was analytically graded.

2.1 Digestion of Clay Samples.

The mined clay was sun-dried for 24 hours and size reduced to fine particles using mortar and pestle. The ground samples were sieved to remove impurities and then oven dried at 105°C. The samples were then put in contact with hydrochloric acid in a 250 cm^3 flask placed in a regulated water bath. The flask was heated while continuously being stirred. At the completion of the heating time, the slurry was removed from the bath and allowed to cool. After the cooling, the slurry was filtered via a Buckner funnel and the clay residue was washed several times with distilled water, followed by filtration until the filtrate was neutral to pH indicator paper.

2.2. Acid Activation of Clay Sample

The acid activation was carried out according to the method described by [18], [19] and, [20]. The clay was ground into powder using pestle and mortar, and sieved through a laboratory test sieve of aperture - 150µm. The clay sample (100g) was introduced into a 600ml Pyrex Beaker and 250ml of 1M Tetraoxosulphate (VI) acid solution added. The mixture was homogenized in a thermostat bath at a temperature of 95^{o}C for 3hours. The resulting mixture was filtered, washed with distilled water severally to reduce the acidity. The activated clay sample was dried in an electric oven at a temperature of 105^{o}C. The dried activated clay sample was then sieved through a laboratory test sieve of aperture - 150µm and stored in an air tight container.

2.3 Characterization of Clay Sample

The clay samples were characterized using Atomic Absorption spectrophotometer and X-ray Fluorensce (PW 4030 X-Ray Spectrophotometer). This is shown in Table1.

PARAMETER	Raw Clay	Bleached Clay
Moisture content %	7.95 ±0.51	6.3
Volatile matter %	2.46 ±0.04	.65
Fixed carbon %	0.84 ±0.08	.52
Specific Gravity g/cm^3	2.57	2.38
pH	5.7	5.6
Bulk density g/cm^3	1.56	0.89
Non Clay Residue (%)	3.55	0.68
TitratableAcidity(mg NaOH/g	0.78	0.46
SiO_2	63.39	63
AI_2O_3	4.42	5.75
Fe_2O_3	0.11	0.01
CaO	1.62	0.54
MgO	2.33	0.5
Na_2O	4.10	0.35
K_2O	3.48	1.25
Ignition loss	11	8.0

Table 1 The physicochemical properties of raw and activated Ngwo Clay..

2.4 Bleaching Process and Analyses

Bleaching of the palm oil was carried out according to the procedure reported by [21]. 50g of degummed, palm oil was poured into a 50ml Pyrex beaker and heated up to a required temperature of 100^oC, for the reaction on a magnetic hot plate. When the magnetic hot plate reached the set temperature, the activated clay sample was added. The process was carried out at 20 -160^oC and the contact times were 10, 20, 30 40 an 50min, with clay dosage of 4%, 6% and 8%. At the end of the process, the mixture was filtered through Whitman No 1 filter paper into a test tube until a reasonable amount was obtained. The absorbance of the oil was measured using a UV spectrophotometer as follows: 0.1g of palm oil was diluted in 7.5ml of petroleum ether and the absorbance of the sample determined at 445nm wavelength using the petroleum ether as reference [21]. The percentage of oil bleached was calculated as follows:

$$\%Bleached = \frac{Absorbance_{unbleached} - Absorbance_{bleached}}{Absorbance_{bleached}} \times 1\,00 \quad \ldots\ldots\ldots\ldots\ldots\ldots\ldots\ldots 1$$

Table 2 The effect of bleach temperature on Colour, PV, AV and FFA of bleached palm oil; time is constant at 40min.

Tables 2nad 3 show the results of characterization experiments on bleached oil.

Temperature ^oC	**Colour in 1 inch cell**		**Peroxide value**	**Anisidine value**	**Free fatty acid**
	Bleached oil	**Deodorized oil**			
20	14.2	3.8	6.5	3.60	0.62
40	13.8	3.7	6.0	3.65	0.60
60	13.5	3.8	5.5	3.70	0.48
80	13.3	3.6	5.0	3.80	0.50
95	12.6	3.5	4.3	3.85	0.40
100	11.5	3.4	3.0	4.05	0.12
110	9.6	3.5	2.8	6.00	0.13
120	9.2	4.8	1.2	6.50	0.40
140	8.5	5.1	1.0	10.50	0.50
160	8.0	5.5	0.9	14.50	0.60

Time(days)	**Colour (red), 1” Cell**		**Peroxide Value of deodorized oil**	
	Bleached at 110^oC	**Bleached at 150^oC**	**Bleached at 110^oC**	**Bleached at 150^oC**
1	3.10	5.8	0.00	0.00
4	3.20	5.9	0.46	1.80
7	3.30	6.2	0.82	2.00
14	3.35	6.8	1.17	2.32
21	3.45	7.4	1.50	2.80
28	3.52	8.6	1.75	3.48

Table 3 The effects of colour and PV on the keeping quality of bleached and deodorized palm oil.

2.5 Experimental Design of Box Benhken Design (BBD)

Box Benhken Design of experiment, also known as (central composite rotatable design) was used to optimize the variables in order to obtain optimum bleaching conditions of palm oil using activated Ngwo clay. Time, temperature and dosage were chosen as independent variables, and the percentage oil bleached was the dependent variable. The experimental range and level of independent variables for bleaching of palm oil were analyzed using BBD. In this study, a set of 20 experiments were carried out. These 20 experiments contain 8 core points, 6 stars like points and 6 null points. The distance of the star like points from core point is given by D = 2n/4, where n is the number of factors (for three factors, D = 2x3/4 The results are shown in table 4**,** where X_1 a coded variable that represents the temperature, X_2 represents the time and X_3 represents the clay dosage.

The design of the experiment was analyzed with the aid of Minitab software. By solving the regression equation and analyzing the response surface contour plots, the optimum values of selected variables were obtained. The most important parameters affecting the efficiency of the bleaching process are *temperature* (X_1), *time* (X_2) and dosage (X_3). In order to study the combined effects of these factors, experiments were performed by varying physical parameters using the experimental design. Experimental and Theoretical values for percentage palm oil bleached were obtained. It can be seen that the optimum percentage oil bleached of 83% was obtained at temperature of about 100°C in 70mins bleaching time and clay dosage of 6grms. The result of analysis of variance (ANOVA) for the response surface quadratic model is determined. The tests for adequacy of the regression models, significance of individual model coefficients and the lack of fit test were performed using the same statistical package. The regression model obtained is given in equation 2.

$$Y(\%) = -35.1 + 1.27X_1 + 2.17X_2 + 25.24X_3 - 0.00621X_1X_2 - 0.207X_2X_3 - 0.124X_1X_3 - 0.0041X_{12} - 0.0197X_{22} - 0.094X_{32} \quad \ldots\ldots 2$$

The P values were used as a tool to check the significance of each of the coefficients, which in turn are necessary to understand the pattern of the mutual interactions between the test variables [22]. The larger the magnitude of F-test value, the smaller the magnitude of P-values and the higher the significance of corresponding coefficient by [23]. When the value of P is less than 0.05, It shows that the model terms are significant. The fitness of the model equation was also expressed by the coefficient of determination, R_2. In this case, X_1, X_2, X_3, X_{12} and X_{22} are the significant model terms. The final mathematical model by eliminating the insignificant terms and interactions is expressed as.

$$Y(\%) = -35.08 + 1.27X_1 + 2.17X_2 + 25.2X_3 - 0.00411X_{12} + 0.0197X_{22} \quad \ldots\ldots 3$$

2.6 Statistical Analysis

A quadratic polynomial equation by Box Behnken Design was developed to predict the response as a function of independent variables and their interaction. In general, the response for the quadratic polynomials is described by equation 4:

$$Y = \beta_0 + \sum(\beta_i X_i) + \sum(\beta i X i)^2 + \sum(\beta_{ij} X_{ij}) \quad \ldots\ldots 4$$

Where Y is the response (yield); β_o is the intercept coefficient, β_i is the linear terms, β_{ii} is the squared terms and β_{ij} is the interaction terms, and Xi and Xj are the un-coded independent variables [24]. Analysis of variance

Exp. Run	Std. value	FACTORA (X_1) mins	FACTOR B (X_2) ^{0}C	FACTOR C (X_3) grms	RESPONSE Y
1	9	50.00	60.00	4.00	35.30
2	13	50.00	80.00	6.00	22.00
3	16	50.00	80.00	6.00	52.00
4	5	30.00	80.00	4.00	59.00
5	17	50.00	80.00	6.00	59.30
6	7	30.00	80.00	8.00	12.20
7	10	50.00	100.00	4.00	70.00
8	8	70.00	80.00	8.00	61.10
9	14	50.00	80.00	6.00	8.00
10	4	70.00	100.00	6.00	83.00
11	6	70.00	80.00	4.00	57.OO
12	3	30.00	100.00	6.00	12.20

(ANOVA) was applied to estimate the effects of main variables and their potential interaction effects on the oil

yield.

Table 4. Experimental Results as obtained from the lab

13	11	50.00	60.00	8.00	8.00
14	15	50.00	80.00	6.00	56.10
15	2	70.00	60.00	6.00	8.00
16	12	50.00	100.00	8.00	12.20
17	1	30.00	60.00	6.00	55.60

2.7 Model Fitting and Statistical Analysis

Results obtained from the experiments (observed and predicted) are summarized as follows:

- The results were used to develop a second order polynomial equation (in coded units) that could relate oil yield to the parameters studied. The following quadratic equation model explained it.

$$\mathbf{Y= 76.68 + 8.79X_2 + 12.44X_3 + 9.06X_4 – 11.77X_{12} – 4.98X_{22} – 5.38X_{32} – 2.78\ X_{42} +3.22x1X_4+3.50X_3...5}$$

- From the experimental design and the experimental results obtained. The second order response functions representing Y is the response for palm oil yield, X_1 the coded value of variable temperature (T), X_2 the coded value of variable ratio methanol to oil (M), X_3 the coded value of variable weight of catalyst (W), and X_4 the coded value of variable reaction time (t). The closer the value of R_2 to unity, the better the empirical models fit the actual data. On the other hand, the smaller the value of R_2, the lesser will be the relevance of the dependent variables in the model in explaining the behavior of variations,[25]. Thus, the predicted values match the observed values reasonably well, with R_2 of 0.94.

III. RESULTS AND DISCUSSION

3.1 Characterization of Ngwo Clay

Table 1 shows the results of the characterization of both raw and activated Ngwo clay . the silicate content of both clays is good showing that it can be a good source of silica in the production of glass , as well as in floor tiles work. The increase from 61.39 tp 63 after activation may be as a result of non solubility of the compound. The other metal oxides were reduced in value, probably because of the clay"s mineral dissolution in the acid.

3.2 Regression model

The three variables that affect the efficiency of bleaching of palm oil using activated Ngwo clay examined in the optimization study were; Temperature, (^oC), Time, (Minutes), and Clay Dosage (%). Central Composite Rotatable Design of Box Benkhen was used in the work. The BBD was used to develop correlation between these operating variables and the efficiency of bleaching. The experimental and predicted values are presented with the complete design matrix in table 4. the quadratic terms were estimated by using the runs at the Center points. Selection of the model was based on the highest order, where the additional terms were significant, and the model was not adjudged insignificant lack of fir, and where the Adjusted R-squared and Predicted R – squared are in agreement, (within 0.2 of each other). The linear model was assumed based on these conditions.

3.3 Design Matrix Using BBD For Palm Oil Bleaching

Table 5 shows the results of the analysis of variance.

Table 5. The Analysis of Variance Table (ANOVA TABLE)

Source	Sum of square	df	Mean Square Value	F-Value	P-Value
Model	7662.04	6	1277.01	4.35	0.0203
A-Time	614.25	1	614.25	2.09	0.01785
B-Temperature	621.28	1	621.28	2.12	0.1762
C-Absorbent Dosage	2041.60	1	2041.60	6.96	0.-248
AB3504.64	1	3504.64	11.95	0.0062	-
AC-647.70	1	647.70	2.21	0.1681	-
BC-232.56	1	232.56	0.79	0.3941	-
Residual	2933.07	10	293.31	-	-
Lack of Fit	810.72	6	135.12	0.25	-
Pure Error	212295.12	4	530.59	-	0.9330
Cor Total	10595.12	16	-	-	-

The relative effects of each of the varaiables to the total variability was interpreted using ANOVA, because total variance of the process is equal to the sum of the component variaces if the factors are acting separately, [26]. ANOVA has its advantage in its use to rank the factors effects on the total variation in order of magnitude. This has effect of showing the points of effort in the variability reduction, so as to maximally improve the process within a minimum time and effort, [27].

The Model F-value of 4.35 implies that the model is significant.There is only a 2.03% chance that a "Model F-Value" this large could occur due to noise.Values of "Prob > F" less than 0.0500 that indicate model terms are significant. In this case C, and AB are significant model terms. Values greater than 0.1000 indicate the model terms are not significant. If there are many insignificant model terms (not counting those required to support hierarchy), model reduction may improve the model. The "Lack of Fit F-value" of 0.25 implies the Lack of Fit is not significant relative to the pure error. There is a 93.30% chance that a "Lack of Fit F-value" this large could occur due to noise.

The "Pred R-Squared" of 0.3807 is in reasonable agreement with the "Adj R-Squared" of 0.5571. "Adeq Precision" measures the signal to noise ratio. A ratio greater than 4 is desirable. The ratio of 7.702 indicates an adequate signal. This model can be used to navigate the design space. This is shown in table 6

The post ANOVA information are shoen in Tanle 7

Table 7 The post ANOVA information

Coeff. Factor	**Estimate**	**Standard Difference**	**95% C.I Error**	**95% C.I Low**	**High**
Intercept	**39.4**	**1**	**4.15**	**30.22**	**48.73**
A-Time	**8.76**	**1**	**6.06**	**-4.73**	**22.25**
BTemperature	**8.81**	**1**	**6.06**	**-4.68**	**22.30**
C-ClayDosage	**-15.98**	**1**	**6.06**	**-29.47**	**-2.48**
AB29Bleaching.60	**Efficiency1 %**	**8.56**	**Actual**	**10.52**	**48.68**		**1**
330.17684			**Optimal point**				
AC12.73	**1**	**8.56**		**-6.35**	**31.80**		**1**
-7.39062			**Time**				
BC7.63	**1**	**8.56**		**-26.70**	**11.45**		**1**
-2.11562			**Temperature**			**Final Equation in Terms of Coded Factors:**	
-8.64375			**Clay Dosage**				
0.074000			**Time - Temperature**				
0.31813			**Time -Adsorbent Dosage**				
-0.19063			**Temperature -Adsorbent Dosage**				

Tables 8 and 9 give the final results in terms of coded and actual factors respectively.

Bleaching Efficiency %	**Coded**
39.47	optimum
8.76	*A
8.81	*B
-15.98	*C

Table 8 Results in terms of coded

29.60	*A*B
12.73	*A*C
-7.63	*B*C

factors

Table 9, Results in Terms of Actual Factors:

Table 10 shows the results of predicted, actual and residual values.

Table 10 Predicted Values, Actual Values And Residuals

Standard order	Actual value	Predicted value	Residual
1	55.56	51.50	4.10
2	8.00	9.82	-1.82
3	12.20	9.92	2.28
4	83.00	86.65	-3.65
5	59.00	59.41	-0.41
6	57.00	51.48	5.52
7	12.20	2.01	10.19
8	61.10	44.98	16.12
9	35.30	39.01	-3.71
10	70.00	71.88	-1.88
11	8.00	22.31	-14.31
12	12.20	24.68	-12.28
13	22.00	39.37	-17.47
14	8.00	39.37	-31.47
15	56.10	39.37	16.63
16	52.00	39.37	12.53
17	59.30	39.37	19.83

3.4 Model Graphs

Normal Plot of Residuals

The normal probability plot indicates whether the residuals follow a normal distribution, in which case the points will follow a straight line. Expect some moderate scatter even with normal data.

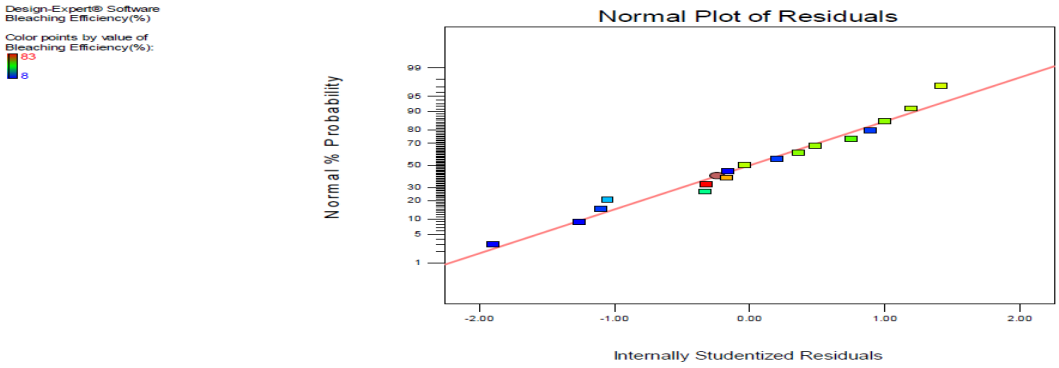

Fig. 1 Normal Plot of Residuals

Residuals vs Predicted Plot

This is a plot of the residuals versus the ascending predicted response values. It tests the assumption of constant variance. The plot should be a random scatter (constant range of residuals across the graph.) Expanding variance ("megaphone pattern <") in this plot indicates the need for a transformation

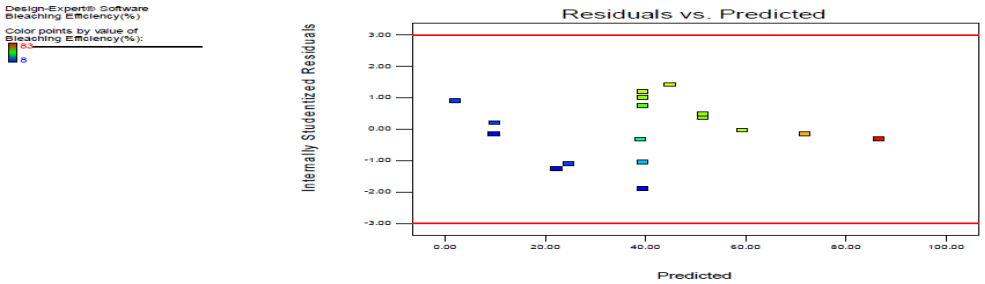

Fig 2 Residuals vs Predicted Plot

Residuals vs Run

This is a plot of the residuals versus the experimental run order. It allows you to check for lurking variables that may have influenced the response during the experiment. The plot should show a random scatter. Trends indicate a time-related variable lurking in the background. Blocking and randomization provide insurance against trends ruining the analysis.

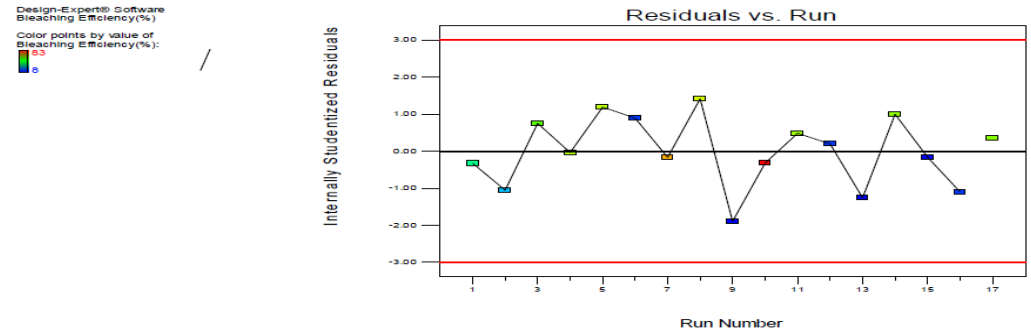

Fig. 3 Residuals vs Run

A graph of the actual response values versus the predicted response values. It helps detect a value, or group of values, that are not easily predicted by the model. The data points should be split evenly by the 45 degree line. If they are not, a transformation comes in (check the Box-Cox plot) to improve the fit.

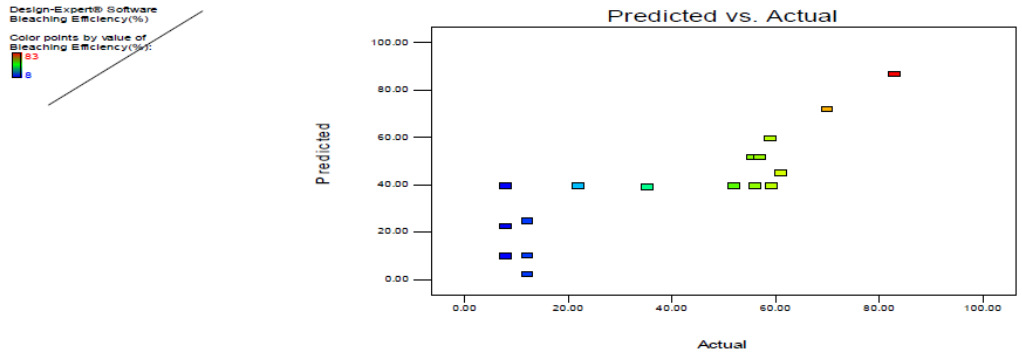

Fig 4 Predicted vs Actual

3.4 Effects of bleaching factors on the bleaching efficiency, (One factor plot)

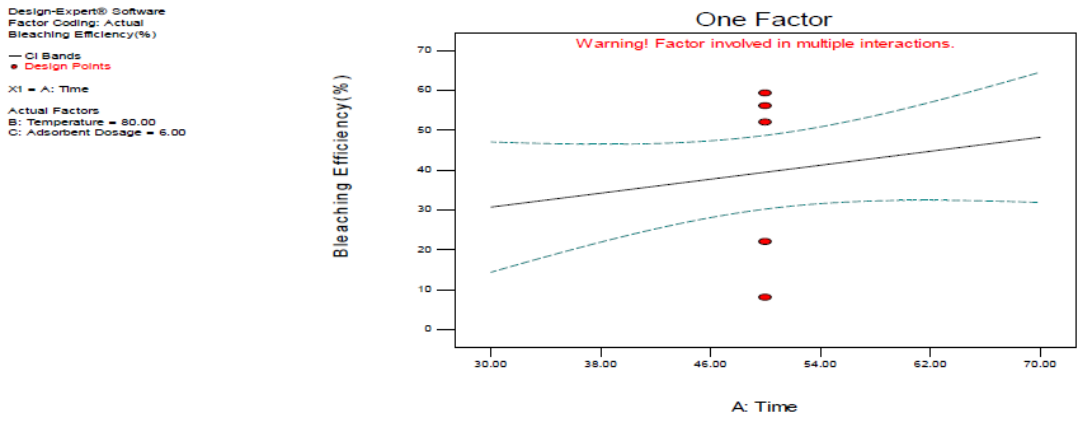

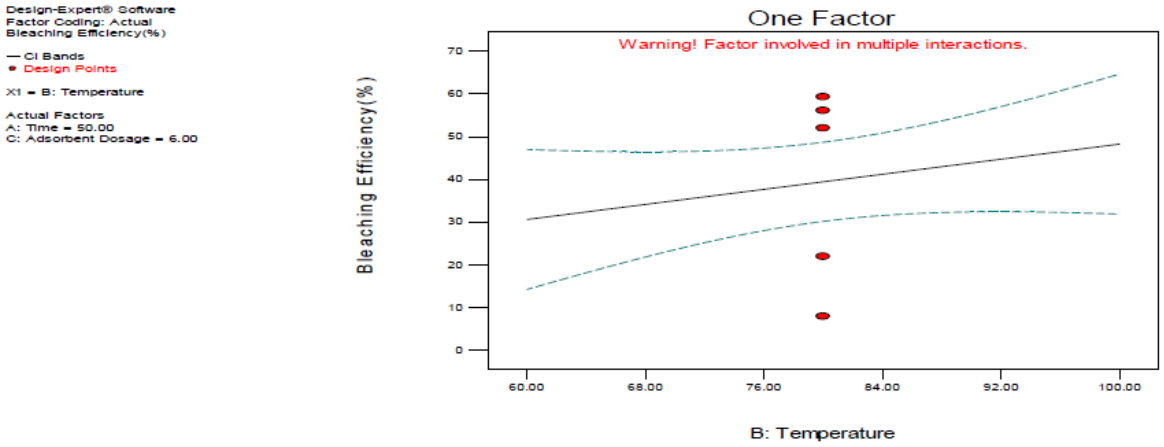

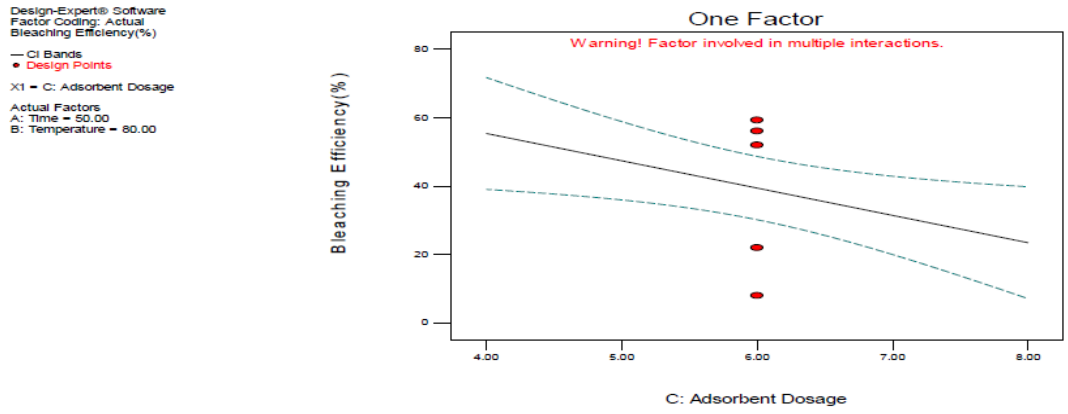

Fig 5 Interactive effect of (a)Time, (b)Temperature, and (c) Clay dosage. (One factor plot)

3.5 Model Graphs: Effects of bleaching factors on the bleaching efficiency, (Two factors plot)

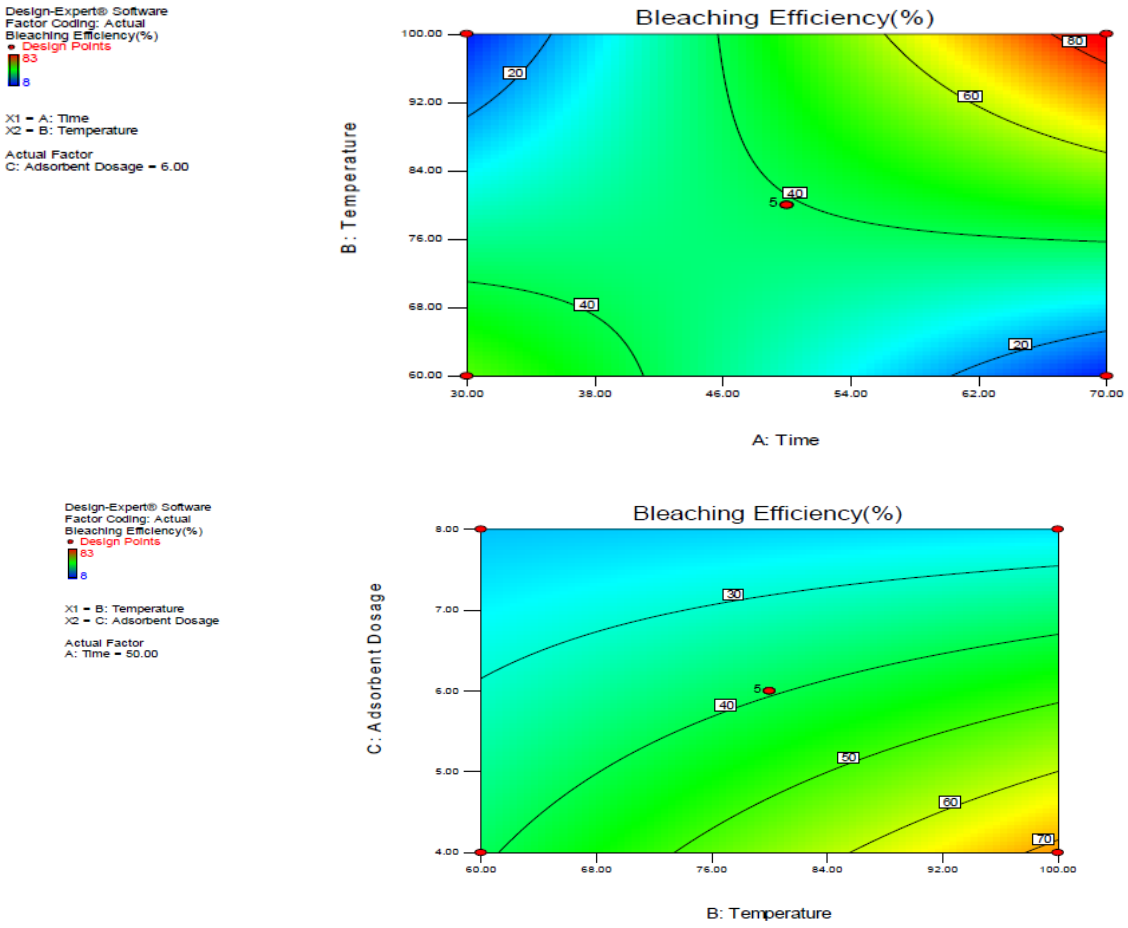

Fig. 6 Interactive effect of (a)Time, (b)Temperature, and (c) Clay dosage. (Two factor plot)

3.6 Contour plot of interaction effects of the factors

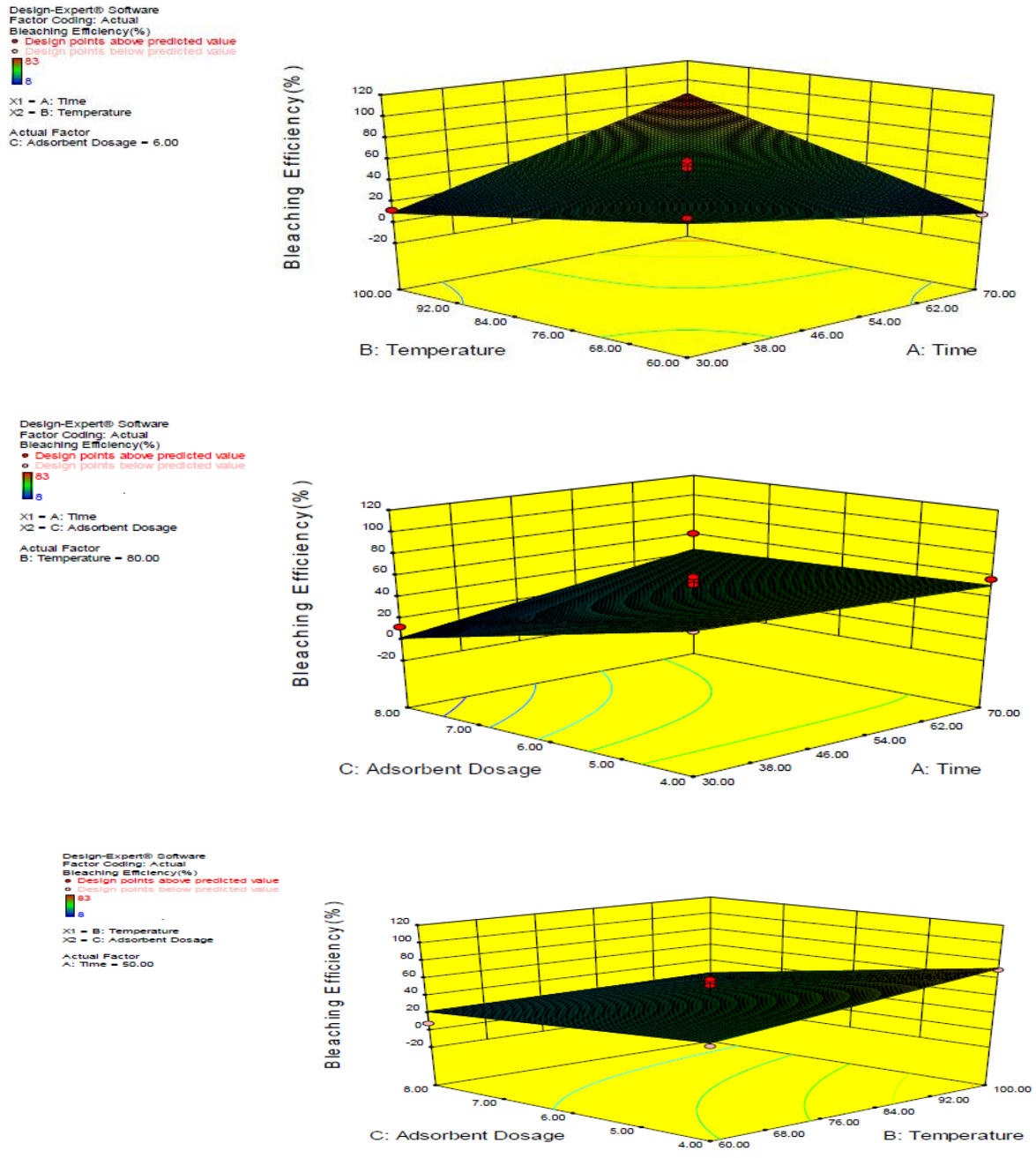

Fig. 7, 3D surface plotof the interaction effect of (a)Time, (b)Temperature, and (c) Clay dosage.

3.7 Effect of Adsorbent Dosage on Bleaching Efficiency:

The clay dosage was varied from 4.0grms to 8.0grams. It was observed that increasing the clay dosage increased the bleaching efficiency. The results clearly indicate that the bleaching efficiency increases to an optimum value at adsorbent dosage of 4.02g, above which further increase in adsorbent dosage has no significant effect on it, but the value remains constant. This could be explained by the fact that adsorption equilibrium has been reached between the adsorbent/oil mixtures, thereby, preventing further pigment removal by the excess adsorbent dosage. Hence, it can be rightly concluded that absorbent dosage of clay is directly proportional to the bleaching efficiency.

3.8 Effect of Temperature on Bleaching Efficiency:
Fig. 5 shows that the bleaching efficiency is favoured by an increase in process temperature. From the figure it is obvious that bleaching does not proceed to any appreciable degree at low temperatures. But as the temperature is increased from 60°C to 100°C, the bleaching efficiency increased showing that temperature promotes access to further adsorption sites in the adsorbent. The bleaching efficiency increased with contact time at high temperature until it reaches a maximum optimum value of 99.84^0C, then it starts to decrease with increasing contact time. These indicate that a further increase in the reaction temperature will not have any or much significant effect on the bleaching efficiency. Hence, temperature varies directly as bleaching efficiency.

3.9 Effect of Time on Bleaching Efficiency:
According to the chart shown above, it is obseved that bleaching does not proceed to any appreciable degree at low contact time or reaction time. But as the time is increased from 30mins to 70mins, the bleaching efficiency increased showing that reaction time favours positively and promotes access to further adsorption sites and decolourization in the adsorbent clay. The optimum time as observed in the study is 39.27min. The bleaching efficiency increased with contact time at high temperature until it reaches a maximum, and starts to decrease with increasing time duration. Consequently, time factor in beaching of palm oil improves bleaching efficiency.

3.10 Optimization
Numerical optimization was applied to search for the design space, and the created model was used to find the factors settings that met the objective of optimal bleaching efficiency. The optimal parameters were selected based on the highest desirability, with 40 minutes, 100^oC, and 4% for Time, Temperature and Clay dosage respectively. This gave an efficiency of 83.39% which has a good correlation with the actual value of 82..39%. Validation was done by repeating the bleaching experiments at the predicted optimum conditions as shown in table 7. The results obtained from the optimization of the bleached palm oil parameters showed that the bleaching efficiency is linearly affected by process temperature and the contact time, and quadratic dependent on adsorbent clay dosage, as these can be interpreted from graph and chart shown above. As process temperature increases, duration of time and clay dosage invariably increase the bleaching or degree of decolourization.

IV. CONCLUSION

The optimal process parameters on the efficiency of activated Ngwo Clay on the bleaching performance of palm Oil has been investigated. Response Surface Methodology was used to study the effect of key parameters of Temperature, Time and Clay Dosage on the bleaching of palm oil. Box Benkhen Design, (BBD), a Central Composite Rotatable Design, with 17 assay, was successfully applied in the experimental design in order to optimize the variables. The conditions foe the optimal bleaching efficiency were found to be; temperature, time and clay dosage of 99.84^oC, 40min. and 4g respectively. This resulted to 80.39 % of palm oil bleached Graphical response surface and contour plots were used to locate the optimum points this study clearly shows BBD as a good technique for studying the effect of major parameters in the bleaching of palm oil. it has also shown that Ngwo clay is a veritable source of adsorbent for bleaching vegetable oils. The good correlation between the predicted and experimental values shows that the method adopted is good enough for the process and that all the process variables of temperature, contact time, and clay dosage were significant.

REFERENCES

[1] S. Parwez, (2006), The Rearson Guide to the B.Sc (Nursing) Entrance Examination. Pearson Education India pp. 109.
[2] E . Bernardini,. (2011), Vegetable oils and fats Processing, Vol.2, interstampa Rome Inc.
[3] D.D. Brooks, (1999), Bleaching Factors that affect the oil loss. Proceedings of the 1999 PROIM. International palm oil congress, (chemistry and technology. 45-51 S.O Egbuna., A.J Ujam and M.E., Ejikeme, (2013), Comparative Analysis of Diffusion Rate in Palm Oil Extraction Using Different Extraction Solvents, ARPN Journal of Science and Technology; Vol.3 No 11, 1076 - 0 1089.
[5] G Borner and M Schneider. (1999), practical Experiences with countercurrent bleaching process. Proceedings of 1999 PORIM international Palm oil congress, (chemistry and technology(52-59
[6] Vov Sonntag, (1979), compsotion and characterization of Individual fits and Oils pp. 289-477
[7] T.L Mahatta (1975), Technology and refining of oils infacts, small business publications (SBP) building and/45 ROOP Nager, New Delhi
[8] A.D., Rich (1964), Basic Factors in Bleaching of fats and oils, J.Am. chemical society, 42, 315
[9] M.K. Gupta (2008), practical guide to vegetable oil processing, (AOCS Press, Urbana, IL).
[10] S.O Egbuna. and N.A.G Aneke., (2005), Evaluation of Quality stability in a physically refined palm oil, proceedings of the 25th AGM of the NSCHE, Kaduna.
[11] P.G. Nutting,., (1975), Adsorbent clay, USA ecological surey Bulletin 928 pp. 127
[12] S.O Egbuna., E Ugadu. and A.J. Ujam (2014), Effect of thermal activation on the physio-chemical properties of white clay a natural local adsorbent. International journal of engineering invention, pp.
[13] F.K. Hymore (1996), Effects of some additives on the performance of a-acid activated clay in the bleaching of palm oil. Applied clay science (10); 379-385.

[14] M Wong,. (1983), quality control in oil refineries. Proceedings of workshop of quality in the palm oil industry 240-245
[15] P.D. Howes, S.H Lim,.D.B Shaw,. T.C.,Soon, P.K Stemp. (1991),Bleaching Earths,Trends and Developments in Bleaching 1991 PORIM. International Palm Oil Conference(Chemistry and technology) 55-75.
[16] S.O. Egbuna Development of Kinetic model for adsorption of carobnoids, on activated clay in the Bleaching of palm oil. International Journal of Engineering and technology Pp 371-380, 2014.
[17] E.M Ejikeme, S.O., Egbuna and P.C.N Ejikeme optimal Performance of Acid Activated Ngwulangwu clay, International journal of Engineering and innovative technology, pp 13-19, 2013.
[18] O. O., James, M.A., Mesubi, F.A., Adekola, E.O., Odebunmi, J.I.D., Adekeye, and R.B. Bale „"Bleaching performance of a Nigerian (Yola) Bentonite. Latin American Applied Research"". 34, 45 – 49, 2008.
[19] P.C.N,Ejikeme E. Ejikeme, and D.O Onwu. "Optimization of process conditions for the concentration of isopropyl alcohol-water solution using response surface methodology". International Journal of Science & Eng. Research, vol. 4, no. 2.". J. Colloid-Inter. Sci., 292, 381–391, 2013
[20] M.A., M.,Vicente – Rodriquez, M Suarez, J.,de Dios Lopes-Gonzalez, and M. A Banares –Munoz, "Characterization, surface area and porosity analyses of the solids obtained by acid leaching of a Saponite. Langmuir", 12, 566 – 572, 1996.
[21] B. J. Nde-Aga, R Kamga, and J. P. Nguetnkam, "Adsorption of palm oil carotene and free fatty acids onto acid activated Cameroonian clays". Journal of Applied Sciences. 7, 2462 – 2467, 2007.
[22] A., Shrivastava, P.,Saudagar., I., Bajaj, and R. Singhal, "Media optimization for the production of U-linolenic acid by cunninghamella echinulata varielegans MTCC 552 using response surface methodology". International Journal of FoodEngineering, 4(2), 1-2. Silva, J. 2008.
[23] Z.Alam, , S.A. Muyibi, , and N. Kamaldin, "Production of activated carbon from oil Palm empty fruit bunches for removal of zinc. Proceedings of Twelfth International Water Technology Conference", IWTC12 2008Alexandria, Egypt, 373-382, 2008.
[24] S.V Ghadge,. And H. Raheman. "Process optimization for biodiesel production from mahua, (Madhuca indica) oil using response surface methodology". Bioresource Technology 97: 379-384, 2006.
[25] W Cao, C .Zhang, P. Hong, and H. Ji,.. "Response surface methodology for autolysis parameters optimization of shrimp head and amino acids released during autolysis". Food Chemistry 109: 176-183, 2008.
[26] G.I.. Onwuka , Food Analysis and Instrumentation Theory and practice. Naphthali Prints Lagos, 2005.
[27] A. G Wilbura,., Food Quality Assurance. The AVI Publishing Company Inc., West Port Connecticut, 1983.

ISSN (e): 2250 – 3005 || Volume, 05 || Issue, 08 ||August – 2015 ||
International Journal of Computational Engineering Research (IJCER)

Effects of Metakaolin Content on Fresh and Hardened Properties of Self Compacted Concrete

Sanjeev Kumar[1], Rinku Saini
[1] Student of M.Tech, RPIIT Karnal,India
[2] Assistant Professor, RPIIT Karnal,India

ABSTRACT
Self-compacting concrete (SCC) is an innovative concrete that does not requires vibration for placing and compaction. SCC has higher powder content and a lower coarse aggregate volume ratio as compared to normally vibrated concrete. If only cement is used in SCC, it becomes high costly, susceptible to be attack and produces much thermal crack. Therefore it is necessary to replace some of the cement by additives like Metakaolin to achieve an economical and durable concrete. Metakaolin (MK) is a pozzolanic material. It is a dehydroxylated form of the clay mineral kaolinite. It is obtained by calcination of kaolinitic clay at a temperature between 500°C and 800°C. Kaolin is a fine, white, clay mineral that has been traditionally used in the manufacture of porcelain. A SSC mix prepaid with the replacement of cement by metakaolin in different ratios (5%, 10%, 15% and 20%). Slump flow and V- Funnel time increase with increase in the percentage of metakaolin and mechanical properties of SCC like Compressive strength, split tensile strength and elastic modulus of SCC decreases with increases in percentage of metakaolin at the age of 7 days and 28 days but increases with increases in percentage of metakaolin at the age of 90 days.

I. INTRODUCTION

The self compacting concrete is that which gets compacted due to its self weight and is deaerated (no entrapped air) almost completely while flowing in the formwork. In densely reinforced structural members, it fills completely all the voids and gaps and maintains nearly horizontal concrete level after it is placed. It consists of same components as conventionally vibrated normal concrete i.e. cement, aggregates, water, additives or admixtures. Self-compacting concrete (SCC) is an innovative concrete that does not requires vibration for placing and compaction. It is able to flow under its own weight, completely filling formwork and achieving full compaction, even in the presence of congested reinforcement. Self-compacting concrete (SCC) offers various advantages in the construction process due to its improved quality, and productivity. SCC has higher powder content and a lower coarse aggregate volume ratio as compared to normally vibrated concrete (NVC) in order to ensure SCC's filling ability, passing ability and segregation resistance. If only cement is used in SCC, it becomes high costly, susceptible to be attack and produces much thermal crack. Okamura was proposed the necessity of this type of concrete in 1986. Study of this type of concrete with fundamental study on the workability of concrete, were carried out by Maekawa and Ozawa at the University of Tokyo.
It is therefore necessary to replace some of the cement by additives, to achieve an economical and durable concrete. This study aims to focus on the possibility of use of Metakaolin to improve the properties of SCC.

II. METHODOLOGY

2.1 Material

Cement: The ordinary Portland cement 43 grade used, conforming to IS: 8112 – 1989. The color of cement was uniform gray with light greenish shade.

2.1.1 Fine Aggregates

The locally available river sand used as fine aggregates of size less than 4.75 mm.

2.1.2 Coarse aggregates

The locally available course aggregates having size 20 mm used. The shape of the course aggregates was rounded.

2.1.3 Fly ash

The fly ash was obtained from 'RAJIV GANDI THERMAL POWER PLANT' Khedar, Haryana

Fig.1 Fly ash

2.1.4 Superplasticizer

Superplasticizer 'Conplast SP 430' was used as a chemical addmexture for concrete.

Fig.2 Superplasticizer

2.1.5 Metakaalin

The metakaolin was obtained from 'ASTRAA CHAMICALS' Chennai. The color of metakaolin was off- white.

Fig.3 Metakaalin

2.1.6 Water

The tab water having pH 6.4 is used in concrete. It was free from suspended solid and organic materials which is good for fresh and hardened properties of concrete.

2.2 Methodology for Concrete mix design

2.2.1 Mix-proportioning system

According to the Japanese SCC-designing method, suggested by Okamura et al. (2000), the mix proportions are determined as follows:

1. Air content is set at 2%, unless air entrainment is required when freeze-thaw resis- tant concrete is to be designed.
2. The coarse aggregate content in concrete, Vg, is limited to 50% of the dry rodded content (Vg,lim) excluding air volume.
3. The fine aggregate volume, Vs, corresponds to 40% of the mortar volume (Vm).
4. The water to powder volume ratio, Vw/Vp, is determined on the basis of paste and mortar tests.
5. The dosage of superplasticizer Sp/p (% of powder weight) is adjusted by a test on fresh concrete, to ensure self-compactability.
6. Finally, tests are performed on trial batches of concrete to finalize the mixture proportions.

There are also some important conditions on applying this method (Takadaetal. 1998):

- The maximum aggregate size is 20mm.
- The border size between fine and coarse aggregates is 5mm.
- The particles finer than 0,09mm are not considered as aggregate but as powder.
- Japanese moderate heat Portland cement is used as a standard powder material.

Table 1.Powder compositions

Powder/mixture[a]	β_p	E_p	Powder/mixture[b]	β_p	E_p
Pc	1,08	0,061	100% pc	1,04	0,048
Pfa	0,59	0,024	85% pc+15% lsp	0,98	0,052
Ggbs	1,10	0,046	70% pc+30% lsp	0,93	0,053
Lsp	0,77	0,037	60% pc+40% lsp	0,91	0,061
pc+1% Sp	0,86	0,034	60% pc+40% pfa	0,92	0,041

Table 2.EFNARC Specification for Mix composition

Mix compositions	
Mix Design	Execute the mix design
	Course aggregate < 50%
	Water powder ratio = 0.8 1.0
	Total powder content = 400 – 600 Kg/m^3
	Sand content > 40% of the mortar (volume)
	Sand < 50% of the paste volume
	Sand > 50% by weight of total aggregate
	Free water < 200 l
	Paste > 40% of the volume of the mix

2.2.2 Trials for Mix Design

For designing the concrete mix proportions, quantities were for casting the specimens for different tests. As per the SCC method of design, by varying the mix proportions the results are obtained. The results are not obtained satisfactory in first trial but it obtained after some changes in proportions.

Table 3.Mix composition of Trial Mix

S.No	Mix	Proportion
1	Course Aggregates (Kg)	600
2	Fine Aggregates (Kg)	850
3	Cement (Kg)	415
4	Fly Ash (Kg)	110
5	Water (Kg)	200
6	Super plasticizer (Kg)	7

Table 4.Mix proportion of SCC mixes

Mixes	Cement (Kg)	MK (Kg)	Fly ash (Kg)	Powder (Kg)	Course agg (Kg)	Fine agg (Kg)	Water (Kg)	SP (Kg)	Total (Kg)
SCCMK0	415	0	110	525	600	850	200	7	2182
SCCMK5	394.5	20.5	110	525	600	850	200	7	2182
SCCMK10	373.5	41.5	110	525	600	850	200	7	2182
SCCMK15	352.75	62.25	110	525	600	850	200	7	2182
SCCMK20	332	83	110	525	600	850	200	7	2182

Where
MK = Metalaolin
SP = Superplasticizer
SCCMK0 = Self-compacted concrete with 0% replacement of cement with metakaolin.
SCCMK5 = Self-compacted concrete with 5% replacement of cement with metakaolin.
SCCMK10 = Self-compacted concrete with 10% replacement of cement with metakaolin.
SCCMK15 = Self-compacted concrete with 15% replacement of cement with metakaolin.
SCCMK20 = Self-compacted concrete with 20% replacement of cement with metakaolin.

Table 5. Specifications of specimen

Specimens	Size of Specimen (mm)	No. of Specimens for each mix	Property Study	Days
Cubes	150 x 150 x 150	9 X 5 = 45	Compressive Strength	7, 28 and 90 days
Cylinder	150 x 300	9 X 5 = 45	Tensile Strength	7, 28 and 90 days

III. RESULTS AND DISCUSSION

3.1 Fresh properties of SCC

The tests of fresh properties like Slump flow test, V-funnel test, L-box test, U-box test are performed and fresh properties of concrete mixes are studied with the partial replacement of cement with metakaolin (5%, 10%, 15% and 20%). When the percentage of metakaolin increases then slump flow diameter decreases and slump flow time increases. Due to the high chemical activity and surface area water demand also be increases. Therefore, it loses its fluidity.

Table 6.Fresh properties of Self compacting concrete

Mix	Slump Flow		L-Box		V-Funnel	U-Box
	Dia. (mm)	T_{50m} (sec)	T_L (sec)	(H_2/H_1) (mm)	T_{10} (sec)	(H_1-H_2) (mm)
SCCMK0	636.35	5.78	16.80	0.875	11.19	7
SCCMK5	632.34	6.38	17.23	0.969	11.32	6
SCCMK10	631.31	6.59	16.85	0.940	12.23	5
SCCMK15	628.89	6.61	17.85	0.971	12.29	5
SCCMK20	626.14	6.77	20.16	0.990	12.35	4

3.2 Mechanical properties:

3.2.1 Compressive strength

The effects of partial replacement of cement with metakaolin (5%, 10%, 15%, and 20%) were carried out in compressive strength. The cubes specimens of size 150mm x 150mm x 150mm was tested on compressive testing machine at the ages of 7 days, 28 days and 90 days of curing. The water- powder ratio was kept constant at 0.36. The test result of 5% to 20% replacement of cement with metakaolin gives more strength at both short and long age.

Table 7.Compressive strength of SCC

Mix	Compressive strength N/mm^2		
	7 days	28 days	90 days
SCCMK0	27.50	34.33	40.80
SCCMK5	27.11	34.70	47.25
SCCMK10	22.62	31.50	43.61
SCCMK15	22.55	29.90	46.01
SCCMK20	22.51	28.60	47.42

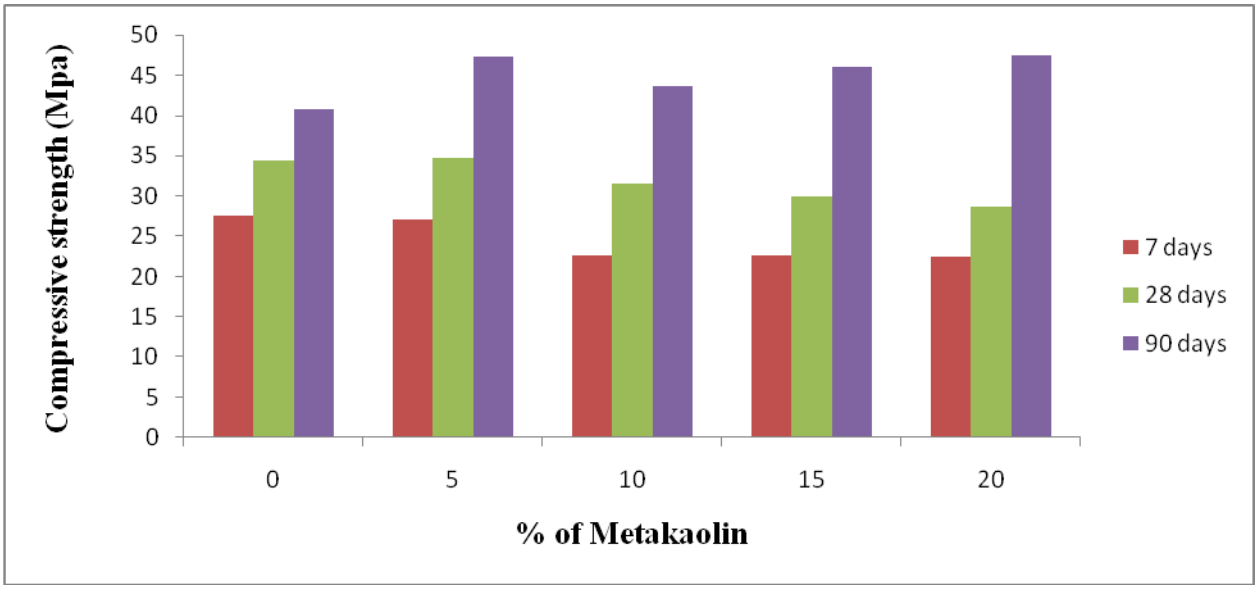

Fig.4 Compressive strength of SCC with metakaolin

3.2.2 Tensile strength test

The effects of partial replacement of cement with metakaolin (5%, 10%, 15%, and 20%) were also carried out in tensile strength. The cylinder specimens of size 150mm x 300mm was tested at the ages of 7 days, 28 days and 90 days of curing.

Table 8.Split Tensile Strength of SCC Mixes

Mix	Tensile strength (N/mm^2)		
	7 days	28 days	90 days
SCCMK0	1.61	1.73	1.83
SCCMK5	1.29	1.6	1.78
SCCMK10	1.25	1.41	1.69
SCCMK15	1.22	1.32	1.7
SCCMK20	0.99	1.31	1.67

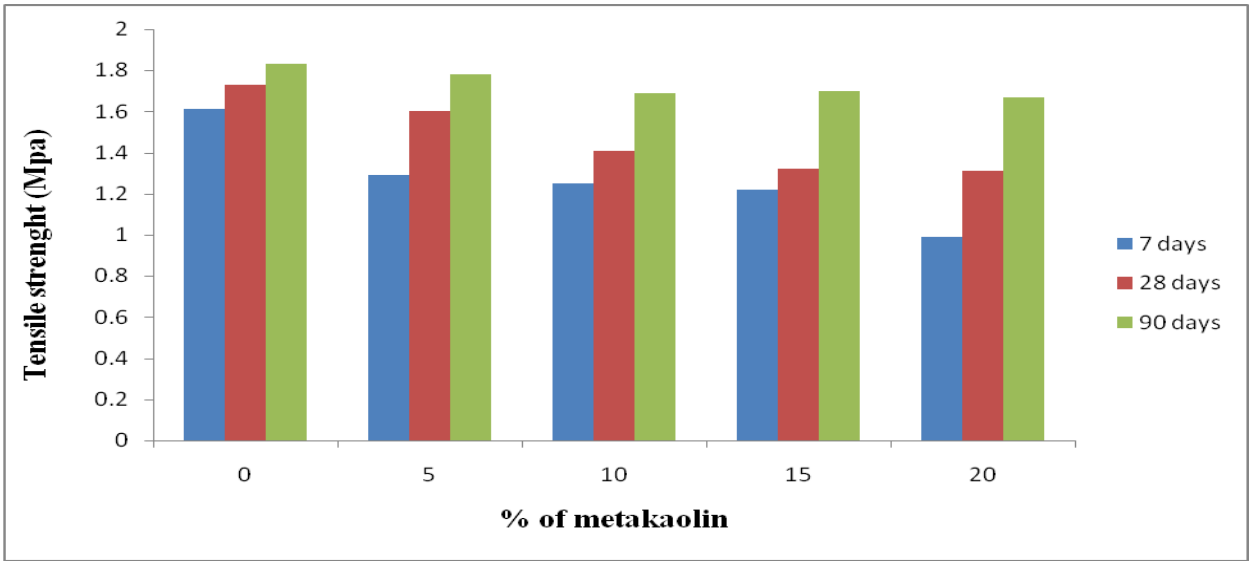

Fig.5 Tensile strength of SCC with % of metakaolin

3.2.3 Ultrasonic Pulse Velocity Test

As per the guidelines of IS: 13311 – 1992, if the velocity is about 4.5 Km/sec, then the quality of concrete is excellent. Velocity criteria for concrete quality grading

Table 9.Ultrasonic Pulse Velocity Test of SCC Mixes

Mix	Velocity (Km/sec)	Quality of concrete	Velocity (Km/sec)	Quality of concrete	Velocity (Km/sec)	Quality of concrete
SCCMK0	5339	Excellent	5631	Excellent	5739	Excellent
SCCMK5	5422	Excellent	5499.52	Excellent	5733	Excellent
SCCMK10	5455	Excellent	5509	Excellent	5734	Excellent
SCCMK15	5332	Excellent	5619.80	Excellent	5710	Excellent
SCCMK20	4919	Excellent	5444.70	Excellent	5677	Excellent

This test is also used for finding the elastic modulus of SCC. As per IS: 13311 (part 1), elastic modulus can be calculated using the equation given below:

$E = \rho (1 + \mu)(1 - 2\mu) V^2/(1-\mu)$

Table 10.Elastic Modulus for SCC mixes

Mix	Elastic Modulus x 10^{10} MPa		
	7 days	28 days	90 days
SCCMK0	6.06	6.74	7.00
SCCMK5	6.25	6.43	6.99
SCCMK10	6.32	6.45	6.98
SCCMK15	6.04	6.71	6.93
SCCMK20	5.14	6.38	6.85

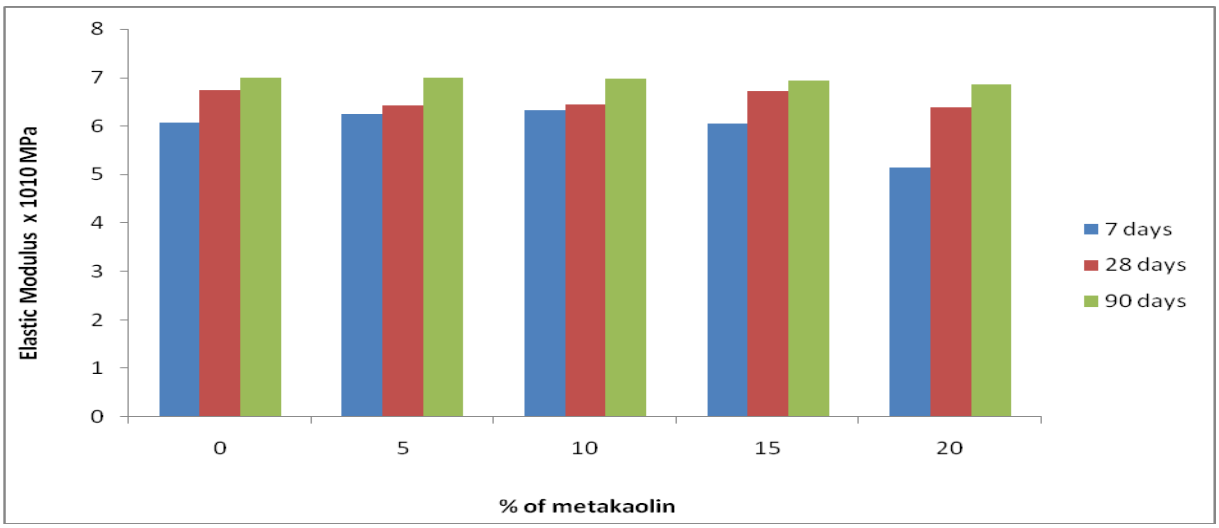

Fig.6 Elastic modulus of SCC with % of metakaolin

IV. CONCLUSIONS

Slump flow time increase with increase in the percentage of metakaolin. Compressive strength of SCC decreases with increases in percentage of Metakaolin at the age of 7 days and 28 days but compressive strength increases with increases in percentage of metakaolin at the age of 90 days. Tensile strength decreases with increases in the percentage of metakaolin at 7 days and 28 days but it observed nearby equal with increases in the percentage of metakaolin at the age of 90 days. The ultrasonic pulse velocity it indicates that quality of concrete is excellent. Elastic modulus of SCC decreases with increases in percentage of Metakaolin at the age of 7 days and 28 days but nearly equal with percentage of metakaolin at the age of 90 days.

REFERENCES

[1] Aiswarya S, Prince Arulraj G, Dilip C. A REVIEW ON USE OF METAKAOLIN IN CONCRETE. IRACST – Engineering Science and Technology: An International Journal (ESTIJ), ISSN: 2250-3498, Vol.3, No.3, June 2013

[2] O.R.Khaleel, H.Abdul Razak. Mix Design Method of self Compacted Meatkaolin Concrete with Different Properties of Caorse Aggregate. July 2013, http://www.elsevier.com/locate/matdes

[3] B. B. Patil , P. D. Kumbhar. Strength and Durability Properties of High Performance Concrete incorporating High Reactivity Metakaolin. www.ijmer.com. Vol 2 Issue 3, May –June 2012, PP-1099-1104. ISSN:2249-6645

[4] Aggarwal, P., Siddique, R., Aggarwal, Y., Gupta, S.M., "Self- compacting concrete – Procedure for Mix Design" Leonardo Electronic Journal. 2008; 12; 15-24.

[5] Dr. Ghalib M.Habeeb, Dr. Mahdi S. Essa. EVALUATION OF METAKAOLIN FOR USE AS SUPPLEMENTARY CEMENTITIOUS MATERIAL.Journal of Kerbala University, Vol 5 No4 Sceintific. December 2007.

[6] P.L. Domone. A Review of the hardened mechanical properties of Self Compacted Concrete. www.elsevier.com/locate/cemconcomp. September 2006.

[7] Brouwers, H.J.H., Radix, H.J., "Self - compacting concrete: Theoretical and Experimental Study". Cement and Research. 2005: 35: 2116- 2136.

[8] P.L.Domone. Self Compacted Concrete: An Analysis of 11 Years of Case Studies. www.elsevier.com/locate/cemconcomp. december 2005.

[9] Specification and Guideline of self compacting concrete, EFNARC, November 2001. www.efnarc.org.

[10] P.K. Mehta. Advancements in concrete technology Concr Inst, 96 (4) (1999), pp. 69–76

[11] S. Iravani, Mechanical properties of high-performance concrete. ACI Mater J, 93 (5) (1996).

[12] Okamura H., and Ozawa, K.: Mix-design for Self-Compacting Concrete, Concrete Library, JSCE, No. 25, pp.107-120, June 1995.

[13] Ouchi, M., Hibino, M., "Development application and Investigation of Self- compacting concrete".

[14] A. Elahi, P.A.M. Basheer, S.V. Nanukutta, Q.U.Z. Khan. Mechanical and durability properties of high performance concretes containing supplementary cementitious materials

[15] Sanjay N. Patil, Anil K. Gupta, Subhash S. Deshpande. Metakaolin- of Mechanical and Civil Engineering (IOSR-JMCE) ISSN: 2278-1684, PP: 46-49 www.iosrjournals.org

[16] O.R Khaleel,S.A A1-Mishhadani and H. Abdul Razak. The Effect of Coarse Aggregate on Fresh and Hardened Properties of Self-Compacting Concrete (SCC). www.elsevier.com/locate/procedia.

[17] Masahiro OUCHI, Makoto HIBINO. DEVELOPMENT, APPLICATIONS AND INVESTIGATIONS OF SELF-COMPACTING CONCRETE

[18] S.N Tande, B.N. Mohite. Application of Self-Compacted Concrete. http://cipremier.com/100032055

[19] Jian-Tong Ding and Zongjin Li. Effects of Metakaolin and Silica Fume on Properties of Concrete. ACI MATERIALS JOURNAL.

[20] IS: 383 – 1970, "Specification for coarse and fine aggregate from natural source of concrete", Bureau of Indian standards, New Delhi, India.

[21] IS: 8112 – 1989, "Specification for 43 grade Portland cement, Bureau of Indian standards", New Delhi, India.